Available online at www.sciencedirect.com
ScienceDirect
Tectonophysics 425 (2006) 159–189
TECTONOPHYSICS
www.elsevier.com/locate/tecto

The structure and timing of lateral escape during the Scandian Orogeny: A combined strain and geochronological investigation in Finnmark, Arctic Norwegian Caledonides

C.L. Kirkland [a,b,*], J.S. Daly [a], E.A. Eide [c], M.J. Whitehouse [b]

[a] School of Geological Sciences, University College Dublin, Ireland
[b] Laboratory for Isotope Geology, Swedish Museum of Natural History, Stockholm, Sweden
[c] Committee on Earth Resources, National Research Council, Keck Centre of the National Academies, NW, Washington, USA

Received 5 April 2006; received in revised form 15 July 2006; accepted 2 August 2006
Available online 14 September 2006

Abstract

Determining the timing, duration and mechanism of tectonic events within an orogenic cycle, such as ocean subduction, continent–continent collision or gravitational collapse, is challenging, especially in ancient orogenic belts. Variations in the tectonic transport direction, however, can be used as a guide to these stages of orogeny. While thrust sheets within the Caledonian allochthon in north Norway were emplaced broadly eastwards perpendicular to the trend of the orogen, many features indicate material transport in other orientations. One dominant feature of the Magerøy Nappe, sitting above and infolded with the Kalak Nappe Complex, is the development of a strong N–S lineation orthogonal to the main transport direction. Strain measurements, in part determined by a new method, are used, in the context of the regional structural data to identify the critical stage in orogeny when compressional forces are balanced by orogen-parallel lateral escape. Quantitative 3-D strain estimation in the Magerøy Nappe indicates prolate deformation with c. 50% horizontal shortening parallel to the thrusting direction (E–W) and c. 200% extension along the orogenic strike (N–S) with c. 30% vertical shortening. Temporal constraint on this fabric is provided by Ar–Ar isotopic analysis of undeformed white mica in cross-cutting granitic pegmatites. These data show that prolate deformation occurred before the white mica cooling age of 416±4 Ma, while the previously determined depositional age of the Hellefjord Schist indicates that it occurred after 438±4 Ma. A granitic pegmatite that intruded the Hellefjord Schist after an initial deformation phase but during or prior to a later deformation, has been dated at 431±2 Ma by U–Pb zircon. A previous lower age constraint on this deformation of 428±5 Ma is given by metamorphic zircon overgrowths on fractured grains. These results constrain the continental collision between Baltica and Laurentia in Finnmark to the interval c. 431–428 Ma. Placed in a regional context, these results indicate that lateral escape was orthogonal to the thrusting direction and occurred during the continent–continent collision stage in the Scandian Orogeny before gravitationally driven collapse.

Keywords: Strain analysis; Geochronology; Scandian Orogeny; Caledonides; Lineation; Lateral escape

1. Introduction

Collisional orogens are a dramatic expression of the dynamic nature of our planet and influence numerous other earth processes including chemical, atmospheric

* Corresponding author. Laboratory for Isotope Geology, Swedish Museum of Natural History, Stockholm, Sweden.
E-mail address: chris.kirkland@nrm.se (C.L. Kirkland).

0040-1951/$ - see front matter © 2006 Elsevier B.V. All rights reserved.
doi:10.1016/j.tecto.2006.08.001

and biological cycles. Orogenic belts reflect the interplay of complex tectonic forces associated with oceanic closure, subduction and collision of plates. Investigating the development of the resulting structural fabrics, quantifying the strains involved and determining the timing of critical stages in orogeny are important elements in charting the evolution of ancient mountain belts.

At its climax, the early to middle Palaeozoic Caledonian mountain belt was probably comparable in length to the present-day Himalayas (Andresen et al., 1998). Hence along strike variations in strain, orientation and timing of contractional versus extensional deformation are to be expected (Chauvet and Seranne, 1994; Krabbendam and Dewey, 1998; Braathen et al., 2000). The Scandian Orogeny is defined as the continental–continental collision between Baltica and Laurentia, involving subduction of the Baltoscandian margin beneath Laurentia (Gee, 1975; Roberts, 2003). The collision between Baltica and Laurentia is considered to have been strongly diachronous, resulting in varying durations of the Scandian event (Hacker and Gans, 2005). In this paper the term "Scandian" is used to refer to the continental collision stage of the closure of Iapetus. At any point within an orogenic system, determining the timing of collision is challenging because the resulting structures are formed progressively by convergent motion as oceanic closure culminates in full-scale continent–continent collision, the likely climax of mountain building. Later structural modifications reflect the influence of gravity-driven forces (Seguret et al., 1989; Alsop et al., 2001). Many structural fabrics within the Scandinavian Caledonides have been interpreted as the result of large-scale lateral convergence resulting in motion predominantly across the regional strike of the belt. However, there are numerous features that preserve evidence of transport directions that are not directed towards the foreland (Braathen et al., 2000). Sequential changes in kinematics as documented by variations in fabric style can sometimes be used to recognise the continental collisional phase of orogeny.

In this paper, strain measurements, in part determined by a new method, are used in the context of the regional structural data to identify the critical stage in orogeny when compressional forces are balanced by the accumulating orogenic mass resulting in orogen-parallel lateral escape. These observations are linked with a series of isotopic age determinations of minerals with clear fabric relationships to delimit the timing of continental collision. The data refine evolutionary models of the region during Caledonian deformation and yield insight into the mechanism and timing of the Scandian Orogeny in northernmost Norway.

1.1. Regional setting

The Scandinavian Caledonides consist of numerous thrust sheets of disparate origins that are classically regarded as being assembled during the early to mid-Palaeozoic. The rocks are grouped into an orogen wide tectonostratigraphic framework of Autochthon, Parautochthon, and Lower, Middle, Upper and Uppermost Allochthons (Roberts and Gee, 1985). The Parautochthon through to the lower part of the Upper Allochthon, are classically considered to have a bipartite subdivision of Baltoscandian basement, and cover sequences of Upper Precambrian and Lower Palaeozoic sedimentary rocks (Roberts, 2003). The contact above the Seve (and correlative Kalak) nappes of the lower part of the Upper allochthons (Zachrisson, 1986) is traditionally regarded as a significant break separating outboard oceanic elements from continental margin sequences deposited on Baltica basement rocks (Andréasson, 1994). However, Kirkland et al. (2006a) have demonstrated Grenville-related deformation and magmatism within correlative rocks in Finnmark, Arctic Norway and Daly et al. (1991), Kirkland et al. (2006a) and Corfu et al. (2005) have dated intrusions of broadly Cryogenian age at higher levels in the same region. This tectonomagmatic history invites a more exotic origin for rocks traditionally regarded as representing the Baltica margin of Iapetus.

Subduction of Baltica beneath Laurentia in the Silurian to Early Devonian (Gee, 1975) led to the successive shortening of diverse units including the Baltoscandian passive margin miogeocline and shelf successions and also more exotic oceanic and arc terranes derived from the Iapetus Ocean including units with Laurentian affinities from the opposite margin (Melezhik et al., 2002; Roberts et al., 2002; Yoshinobu et al., 2002).

Various phases in the destruction of the Iapetus Ocean are charted by several pluses of magmatic activity associated with characteristic plate tectonic settings (Stel-tenpohl et al., 2003). The earliest of these at about 500–480 Ma is linked with the development of ophiolites and island arcs (Dunning and Pedersen, 1988; Pedersen and Furnes, 1991). Between 480 and 450 Ma, magmatic activity is typically envisaged as occurring in continental arcs on the Laurentian margin and is now preserved in the Upper and Uppermost Allochthons (Nordgulen et al., 1993; Yoshinobu et al., 2002). During the waning stages of the Iapetus Ocean between 445 and 435 Ma, when it was a narrow seaway, just before continental collision, an extensive pulse of mantle-influenced magmatism took place. Granitic and gabbroic bodies of this age are prevalent in the Magerøy Nappe, in Finnmark (Vaasjoki and Sipila, 2001; Andréasson et al., 2003; Kirkland et al.,

2005a; Corfu et al., 2006). This event has been associated with the development of short-lived back arc basins produced due to slab roll back as continental–continental collision approached (Pedersen et al., 1992; Andréasson et al., 2003; Kirkland et al., 2005a), although some authors consider it to be related to subduction of a spreading ridge (Northrup, 1997; Corfu et al., 2006). After this phase of magmatism, crustal derived melts accompanied thrusting and tectonic thickening during the main collisional phase. Generally this is considered to have occurred around 425–400 Ma (Roberts, 2003). The final phase of activity in the orogenic cycle is recorded at 405–370 Ma associated with the gravitational collapse and exhumation of the orogen (Ramberg, 1980; Chauvet et al., 1992; Fossen and Dunlap, 1998; Osmundsen et al., 2003).

The Kalak Nappe Complex (KNC), composed of several individual nappes and imbricate stacks, dominates much of Finnmark (Roberts, 1985; Fig. 1). Caledonian events affecting the KNC have traditionally been divided into an earlier Finnmarkian (540–490 Ma) and later Scandian (400–425 Ma) phases or orogenies. Early research in the region ascribed most of the compressional deformation to the Finnmarkian (Sturt et al., 1978). This was based on tectonic fabrics being truncated by mafic igneous bodies of the Seiland Igneous Province (Robins and Gardner, 1975), at the time thought to be around 540 Ma, based on Rb–Sr dating of associated felsic veins and dykes (Sturt et al., 1978). However, recent dating shows the SIP to have been emplaced at c. 560 Ma (Roberts et al., 2004).

Much deformation in Finnmark occurred during the Scandian (Krill and Zwaan, 1987; Dallmeyer, 1988; Krill et al., 1988; Dallmeyer and Reuter, 1989). The c. 438 Ma Hellefjord Schist (Kirkland et al., 2005a) within the Magerøy Nappe is infolded with the KNC demonstrating a deformation phase during or after c. 438 Ma. This is consistent with numerous mineral ages in both the KNC and Magerøy Nappe (Fig. 1) indicating tectonometamorphism at c. 438 Ma and later overprinting at c. 430–420 Ma (Dangla et al., 1978; Kirkland et al., 2006b). Therefore transport in the KNC occurred, at least to some extent, during Caledonian events (Andersen et al., 1982; Dallmeyer and Reuter, 1989). However, the development of a Neoproterozoic mobile belt within the KNC illustrates a protracted Precambrian history, which itself involved several orogenic phases and the construction of an exotic accretionary orogen (Kirkland et al., 2006a). This mobile belt only later docked with Baltica (Kirkland et al., 2006a).

The Upper or Uppermost Allochthon is represented in Finnmark by the Magerøy Nappe. The Magerøy Nappe is recognised as a Scandian structure (Henningsmoen, 1961; Krill et al., 1988) and is considered to overlie the KNC (Krill et al., 1988; Andersen, 1989; Binns, 1989; Kirkland et al., 2005a; Corfu et al., 2006). The Magerøy Nappe cannot have been affected by tectonic events older than the Llandovery, as its deposition is dated at c. 438 Ma by fossil and isotopic evidence (Krill et al., 1993; Kirkland et al., 2005a).

1.2. Stratigraphic setting

The metasediments of the KNC are classically interpreted as belonging to a single conformable sequence consisting, at the base, of proximal psammites and progressively reflecting deposition in a more distal shelf setting (Ramsay, 1971). However, carbonate chemostratigraphy on the Falkenes Limestone (Fig. 1), detrital zircon geochronology and Sm–Nd isotopic data demonstrate the presence of at least three tectonostratigraphic packages in the KNC, namely Svaerholt Succession (980–1030 Ma), Sørøy Succession (840–910 Ma), and Falkenes–Åfjord formations (710–760 Ma; Kirkland et al., in press; Slagstad et al., 2006). These previously juxtaposed lithostratigraphic units were possibly brought together with the Magerøy Nappe during the Scandian Orogeny (Fig. 1).

The Silurian metasedimentary succession in the Magerøy Nappe is subdivided into a basal Kjelvik Group of pelite and greywacke overlain by the Nordvågen Group composed mainly of pelite and minor amounts of limestone, quartzite, conglomerate and greywacke (Andersen, 1981; Andersen, 1984). The Juldagnes Formation of the Nordvågen Group is likely a correlative of the Hellefjord Schist (Kirkland et al., 2005a).

The Hellefjord Schist outcrops extensively in northeast Sørøy and above the Havvatnet Imbricate Stack on Porsangerhalvøya and has been re-assigned to the Magerøy Nappe (Kirkland et al., 2005a) from its original position at the top of the KNC. The Hellefjord Schist consists of purple phyllitic schist and grey psammite, the latter reflecting deep-water turbidites (Roberts, 1968). Some psammites contain volcaniclastic material including zircons that have been used to establish the Silurian (c. 438 Ma) age of the sequence (Kirkland et al., 2005a). Kirkland et al. (2005b) concluded that the Hellefjord Schist has a Laurentian affinity, based on the age of magmatism which associated the Hellefjord Schist to a position within the Upper or Uppermost Allochthon as well as its juvenile Sm–Nd isotopic signature (Binns, 1989; Aitcheson, 1990; Kirkland et al., 2005a). Magmatism of similar age is also present in the Juldagnes Formation on Magerøy (Corfu et al., 2006). A Laurentian

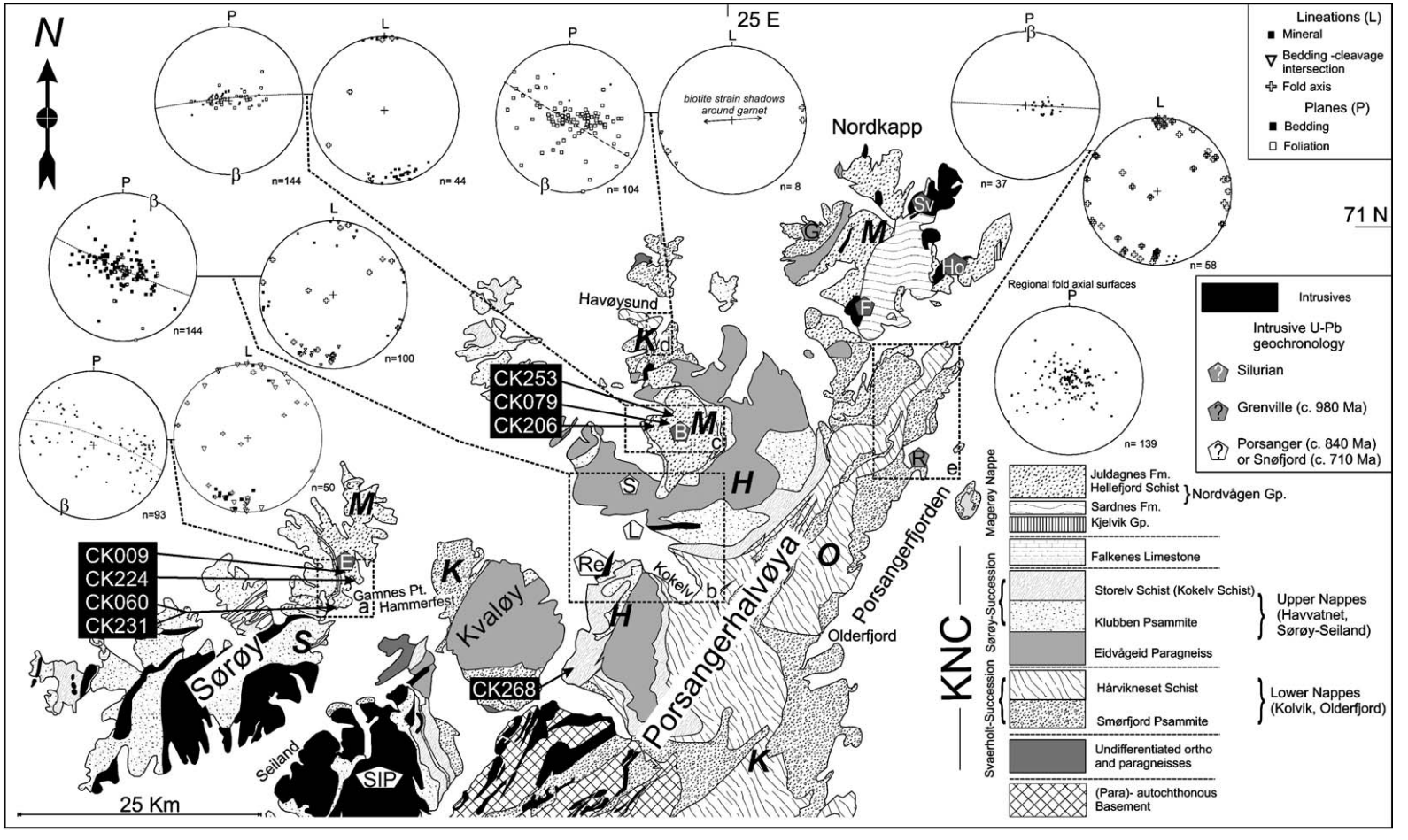

Fig. 1. Geological map of north-western and central Finnmark based on Siedlecka and Roberts (1996) and Kirkland et al. (in press). Lower nappes of the Kalak Nappe Complex (KNC): K = Kolvik, O = Olderfjord; upper nappes: H = Havvatnet Imbricate Stack, S = Sørøy–Seiland and M = Magerøy based on Gayer et al. (1987). Structural study regions (a–e) denoted by dashed boxes corresponding to two stereonets (P = planes; L = lineations). Note dominant N–S lineations in Hellefjord Schist (areas a and c) and both E–W and N–S lineations in other study regions. Beta axes of planes are generally orthogonal to the generally eastward thrusting direction. Granites and migmatites: R = Repvåg, G = Gjesvær, L = Litlefjord, Re = Revsneshamn, B = Bakfjord, F = Finnvik, Sv = Skarsvåg. Gabbroic complexes: Ho = Honningsvåg, SIP = Seiland Igneous Province. Sample CK268 is from the Storelv Schist, others are from Hellefjord Schist. CK060 is the strain study sample. Sample CK079 has been dated by U–Pb geochronology.

affinity for the Hellefjord Schist is also consistent with Sr isotope chemostratigraphy that associates the underlying Falkenes limestone to the Uppermost Allochthon (Slagstad et al., 2006). The pelagic nature of the majority of the Hellefjord Schist indicates that it was deposited in a moderately deep marine setting, with episodic input of volcaniclastic material. Volcaniclastic sedimentation is characteristic of convergent plate margins in marine forearc and back arc settings (Dickinson, 1976; Miller, 1989) and is thus consistent with the palaeogeographic and tectonic setting envisaged for these rocks, deposited in the closing Iapetus Ocean in the early Silurian (Kirkland et al., 2005a).

An intensely deformed conglomerate occurs on western Sørøy near the base of the Hellefjord Schist, which Roberts (1968) interpreted as a slump deposit. A sample from this conglomerate unit has been used in this study to determine the bulk strain (see below) and to constrain the age of deformation by dating undeformed minerals from cross-cutting pegmatites.

1.3. Existing constraint on the age of early Palaeozoic deformation in Finnmark

Scandian deformation in Finnmark resulted from ESE/E-directed compression and is conventionally thought to have occurred at c. 411±7 Ma (Andersen et al., 1982). This constraint is based on the Rb–Sr age of the supposedly syn-orogenic Finnvik granite in the Magerøy Nappe and the Rb–Sr 410±28 Ma age of metamorphism of the Gjesvær migmatite within the KNC (Andersen et al., 1982). The Finnvik granite has recently been re-dated by the U–Pb method and yields an age of 438±2 Ma (Corfu et al., 2006). New Ar–Ar, Rb–Sr and Sm–Nd geochronology, in some cases on individual fabric domains, suggests a more complicated Caledonian history rather than a single Silurian event (Kirkland et al., 2006b). This indicates at least two discrete events— one at c. 438 Ma and a later overprinting event at or before c. 428 Ma (Kirkland et al., 2006b). These two phases of deformation and metamorphism are recorded within the Hellefjord Schist of the Magerøy Nappe and also within the KNC itself. In the Hellefjord Schist an initial phase of deformation and metamorphism at c. 438 Ma was coeval within analytical resolution with penecontemporaneous deposition and magmatism (Kirkland et al., 2005a; Corfu et al., 2006). Mineral cooling ages at a similar time are also recorded in the KNC (Kirkland et al., 2006b). This similarity in ages between the KNC and Magerøy Nappe has been interpreted to indicate a common subduction zone system affecting both (Kirkland et al., 2006b). An amphibole Ar–Ar age of 423±8 from the Engesfjellet granite cutting the Hellefjord Schist implies thrusting of the Magerøy Nappe onto the KNC prior to this time (Kirkland et al., 2006b). Cooling after the Scandian collision is dated by Ar–Ar muscovite ages in the KNC at c. 422 Ma and Ar–Ar biotite ages in the Hellefjord Schist at c. 403 Ma (Dallmeyer, 1988; Kirkland et al., 2006b). In this paper Scandian deformation is shown to be responsible for imposing prolate deformation onto these rocks and its timing precisely constrained.

2. Structural history of the KNC and Magerøy Nappe

In the following account, deformation events are numbered sequentially, in addition, superscripts K and M refer to deformational structures and events recorded within the KNC and the Magerøy Nappe respectively.

It is important to review the form of pre-Scandian fabrics within the Kalak Nappe Complex (KNC) as the geometry of these structures controlled the nature of Scandian fabrics. Initial structural analysis of the KNC was made by Gayer and Roberts (1971) and revised by Gayer et al. (1985) who described a five-phase deformation sequence. $D2^K$ produced recumbent isoclinal folds with $D3^K$ events forming tight to open, gently inclined folds. Later fold phases $D4^K$ and $D5^K$ were described as forming various upright open folds with generally greater wavelengths (Fig. 2).

2.1. $D1^K$–$D2^K$ pre-Scandian events in the KNC

Rice (1987) simplified the deformation scheme into four phases. Rice's $D1^K$ corresponded to an $S1^K$ fabric in garnet porphyroblasts within metabasites (Gayer et al., 1984; Gayer et al., 1987). Daly et al. (1991) described an early biotite foliation folded by $F2^K$ folds. $D2^K$ structures have been regionally correlated from Sørøy onto Porsangerhalvøya (Daly et al., 1991) although several authors emphasized diachroneity in the timing of deformation (Rice, 1984; Chapman et al., 1985). Cross-cutting relationships between intrusives and early structures are preserved in rare cases where the Caledonian strain is low. Dating of these in the lower nappes, combined with detrital zircon analyses, revealed that Grenvillian deformation affected the Svaerholt Succession before 976±3 Ma and after c. 1030 Ma (Kirkland et al., 2006a, in press, Fig. 1). Metasediments in the upper two nappes (Havvatnet and Sørøy–Seiland) have been assigned to the Sørøy Succession (Fig. 1) and were deposited after the Grenvillian deformation event affecting the Svaerholt Succession (Kirkland et al., 2005b, 2006a). Within the Havvatnet Nappe, deformation took

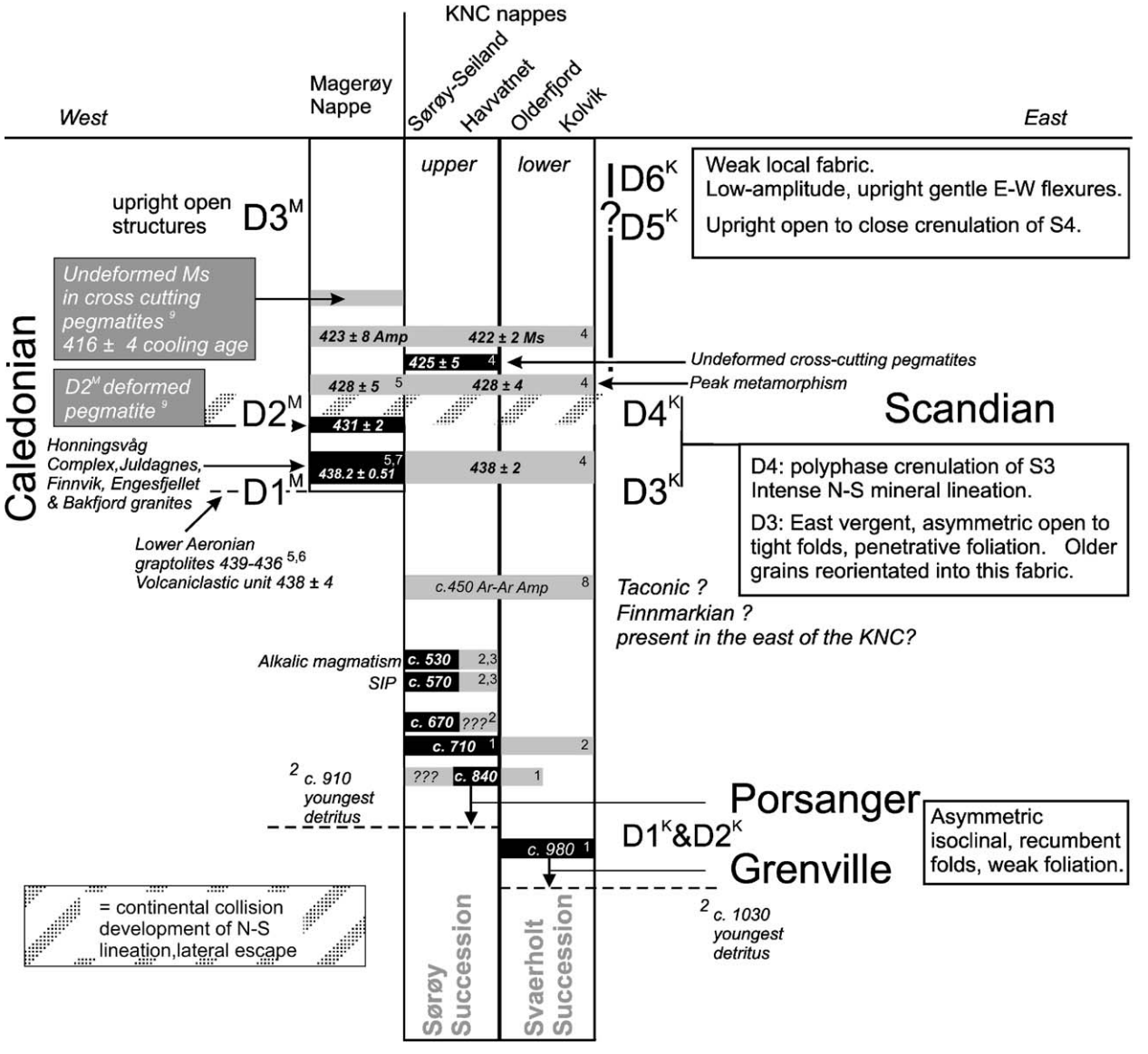

Fig. 2. Temporal and structural chart of deformation within the Kalak Nappe Complex (KNC) and overlying Magerøy Nappe. Black boxes refer to magmatic and grey boxes to metamorphic events. Ages and associated 2σ errors in Ma are given as italicised numbers with cited references denoted as superscripted numerals: 1=Kirkland et al. (2006a), 2=Kirkland et al. (in press), 3=Roberts et al. (2004), 4=Kirkland et al. (2006b), 5=Kirkland et al. (2005a), 6=Krill et al. (1993), 7=Corfu et al. (2006), 8=Dallmeyer (1988), 9=this paper. Mineral abbreviations: Amp=amphibole, Ms=muscovite.

place between c. 840 and 910 Ma whereas in the overlying Sørøy–Seiland Nappe of the KNC, syn-kinematic migmatitic leucosomes in the Eidvågeid paragneiss are dated at 709±4 Ma (Kirkland et al., 2006a). This age is identical to metamorphic overgrowths on zircon in the underlying Havvatnet Nappe. Hence juxtaposition of these nappes occurred at or before c.710 Ma and must predate the Caledonian Orogeny (Kirkland et al., 2006a). These spatial and temporal patterns of granite intrusion and deformation are consistent with terrane accretion from Grenvillian times up to the emplacement of the Seiland Igneous Complex. This prohibits regional correlation of similar early structures across nappe boundaries (Fig. 2).

Following this protracted Neoproterozoic history, later deformational events (e.g., at or before c. 450 Ma; Dallmeyer, 1988), are recorded in some mineral systems within the KNC (Dallmeyer, 1988; Corfu et al., 2004; Kirkland et al., 2006b). However, no clearly-identifiable fabrics can be assigned to these events, perhaps as a result of severe Scandian reworking.

2.2. $D1^M$–$D3^K$ c. 438 Ma deformation; Caledonian ocean closure

$D3^K$ deformation within the KNC occurred at or shortly before c. 438 Ma and is documented through numerous Ar–Ar muscovite ages from grains subsequently reoriented by later deformation (Kirkland et al., 2006b, Fig. 2). However, macroscopic $F3^K$ folds cannot be confidently differentiated from $F4^K$. The age of the $D3^K$ tectonometamorphic event matches that of the $D1^M$ deformation recorded in the Magerøy Nappe and is essentially contemporaneous with deposition of this nappe (Kirkland et al., 2005a; Corfu et al., 2006 Fig. 2). Unlike the Neoproterozoic fabrics within the KNC, that cannot be correlated between nappes (Kirkland et al., 2006a), deformation events from $D3^K$ onwards can be correlated between the Magerøy Nappe and the KNC.

Juxtaposition of the Magerøy Nappe with the KNC is associated with top-to-the-east movements along many of the bounding thrusts (Rice, 1984, Fig. 3) and is usually denoted as $D3^K$. This event is typically assumed to represent the Scandian collision (Sturt et al., 1978; Rice, 1984; Gayer et al., 1985). However, because deformation at c. 438 Ma ($D3^K$) is recorded within both the Hellefjord Schist and the KNC (Kirkland et al., 2006b, Fig. 2), in this paper Scandian events are re-assigned to $D4^K$. The c. 438 Ma ($D3^K$) event cannot represent continent–continent collision because back arc basin extensional magmatism and sedimentation was occurring at this time (Vaasjoki and Sipila, 2001; Andréasson et al., 2003; Kirkland et al., 2005a). Thus the $D1^M$/$D3^K$ structures formed during ocean closure but prior to continental collision.

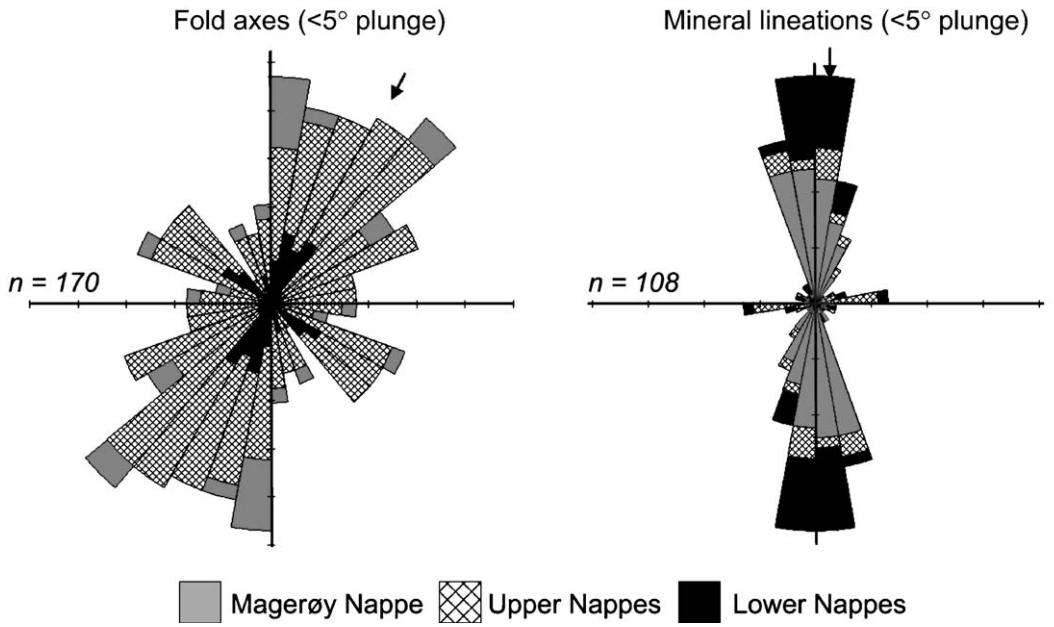

Fig. 3. (a) Fold axis orientations from a regional dataset classified by nappe (Magerøy Nappe and the upper and lower nappes of the Kalak Nappe Complex). The dominant NE–SW trend is orthogonal to bulk compression, unless fold axes in high strain zones have rotated towards the thrusting direction. (b) Mineral lineations have a pervasive N–S orientation associated with constrictional strain interpreted to be due to continental collision, constriction and lateral escape. An E–W trend is also evident in the upper nappes associated with top to the east tectonic transport. Divisions=10 measurements.

The $D1^M$ phase within the Magerøy Nappe (Fig. 2) formed overturned to recumbent folds (Andersen, 1981) and was followed by a deformation phase ($D3^M$) that produced a large upright N-trending synform that largely controls the present geometry of fabrics on Magerøy (Andersen, 1981). Fabric relationships between granites, gabbros and country rocks have been considered to indicate that c. 438 Ma intrusives in the Magerøy Nappe were emplaced in the late stages of $D1^M$ (Corfu et al., 2006). The Finnvik Granite intruded Llandovery sediments and cross cut $D1^M$ structures at c. 438 Ma (Andersen, 1981; Robins, 1998; Corfu et al., 2006). Apophyses from the granite were subsequently folded during $D2^M$ (Andersen et al., 1982). Locally, $D2^M$ structures in the form of recumbent east verging folds affect the c. 438 Ma Engesfjellet and Bakfjord granites which intrude the Hellefjord Schist imparting a strong L–S fabric onto these rocks (Kirkland et al., 2005a). Granitic dykes and sills on Magerøy have been separated by Kjærsrud (1985) into early and late generations, the early set containing an intense $S1^M$ foliation. One of these sills close to the Magerøy Thrust has been dated at 438±3 Ma (Kirkland et al., 2006b) and indicates that folding and foliation must have occurred at c. 438 Ma. Both $D1^M$ and $D2^M$ are likely part of a continuum of deformation that opened and rapidly closed back arc basins early in the convergent history and later culminated in continent–continent collision— the Scandian Orogeny *sensu stricto* (Fig. 2).

2.3. $D2^M$–$D4^K$ the Scandian collision

The N–S trending $D2^M$ fabric has been interpreted in terms of orogenic buttressing and lateral escape concomitant with continental collision (Kirkland et al., 2005a) and must have occurred after c. 438 Ma and the $D1^M$ deformation event (Figs. 1 and 2). Some constraint on the timing of the continental collisional stage ($D2^M$/$D4^K$) is provided by ion microprobe dating of metamorphic zircon overgrowths that heal fractured igneous zircon grains in the c. 438 Ma Bakfjord Granite (Kirkland et al., 2005a). These zircon crystals are fractured and extended parallel to the intense regional N–S $D2^M$ lineation. U–Pb dating of these crystals brackets the $D2^M$/$D4^K$ deformation between c. 438 and 428 Ma (Kirkland et al., 2005a). The $D2^M$ deformation described here is broadly the equivalent of $D1^b$ of Andersen (1981).

Evidence for thrust displacement vectors has been discussed by Townsend (1987), who concluded that the earliest movement was SE-directed while later more brittle movements were eastward (Fig. 3). A decrease in metamorphic grade from garnet–biotite grade (c. 500 °C) to chlorite grade (c. 300 °C) has been linked to this change in transport direction (Townsend, 1986). Within the Laksefjord Nappe Complex, beneath the KNC, lineations also indicate south-eastward transport (Chapman et al., 1979). Later more brittle movements in the Laksefjord Nappe Complex associated with imbrication were also more eastward directed (Williams et al., 1984).

Within Porsangerhalvøya, $D4^K$ formed tight, recumbent top to the east folds (Rice, 1984; Gayer et al., 1985). The $D4^K$ deformation is associated locally with an ESE–WNW to E–W mineral lineation, principally defined by biotite and amphibole. Rotated fold axes, some of which have a sheath-fold geometry, are broadly NW–SE. This is consistent with early ductile SE-directed transport before easterly transport (Figs. 2 and 3). The eastward orientation of $D4^K$ transport is reflected in the alignment of fabric elements within the Havvatnet Imbricate Stack, on Porsangerhalvøya. For example, the orientation of the Litlefjord granite body is rotated into the E–W transport direction within a nappe culmination (Kirkland et al., 2006a; Fig. 1). Though, it is important to note that mineral lineations may not always be of value in determining the transport direction if the deformation deviates from simple shear.

A N–S mineral lineation, usually defined by biotite and amphibole, is the more dominant fabric in many locations within both the KNC and Magerøy Nappe. Fold axes range from sub-parallel to the N–S mineral lineation trend to 30° clockwise from it (Fig. 3). We attribute the N–S mineral lineation also to $D2^M$–$D4^K$ deformation. The timing, kinematics and strain magnitude of the deformation responsible for the N–S mineral lineation is investigated in this paper.

Evidence of broadly N-directed movement within the KNC has been found by Rice (1984), who described thrust fault plane lineations created by garnets within a metabasic dyke gouging striations into the enclosing psammite with a dominant orientation of 07–331°. Similar garnets near Havøysund (Fig. 2) have yielded a Sm–Nd isochron age of c. 436 Ma with hydrothermal zircon in a related quartzofeldspathic vein yielding an age of 428±4 Ma (Kirkland et al., 2006b). Associated strain shadows of biotite around the Havøysund garnets are orientated broadly E–W, parallel to the mineral lineation in the surrounding country rock. If the garnets at both localities are the same age, an east–west constrictive regime at c. 436 Ma or later is implied. This suggests that N-directed transport affected the KNC after c. 436 Ma in keeping with the post c. 438 Ma constraint on the N–S fabric within the Bakfjord granite in the Magerøy Nappe (Kirkland et al., 2005a).

3. Strain analysis

An L–S tectonite conglomerate at Gamnes point on Sørøy within the Magerøy Nappe near the base of the Hellefjord Schist (sample CK060; Fig. 1) has been sampled to determine the strain associated with the $D2^M$ event (see petrographic description in Appendix A). Biotite clots from this sample, aligned N–S within an intense foliation (Fig. 4A), yield Ar–Ar cooling ages of 401 ± 7 Ma (Kirkland et al., 2006b) thus $D2^M$ deformation must have occurred before c. 400 Ma (Kirkland et al., 2006b) and after the deposition of the Hellefjord Schist at c. 438 Ma (Kirkland et al., 2005a). Further constraint on this fabric is provided by dating minerals in undeformed cross-cutting pegmatites as well as $F2^M$ deformed pegmatites.

Sample CK060 is composed of a monomict population of psammite clasts making up c. 20% by volume of the rock. Clasts are up to 65 mm in *X* dimension (Fig. 4B), with a unimodal size distribution (mode of 1.2 mm^2) on the *XZ* principal plane. The matrix is also composed of psammite, making the clasts ideal bulk rock strain markers. There is a well-developed foliation within the rock, primarily defined by biotite. The clasts are all elongated in a N–S orientation parallel to the regional mineral lineation within the Hellefjord Schist on NE Sørøy (Fig. 1) and also within other nappes on Porsangerhalvøya. Occasional locally-developed thin (>1 cm wide) pegmatitic veins and spatially associated garnet are elongated parallel to the *X* orientation of the clasts (Fig. 4C). The garnet is extensively fractured with dislocation planes running at 45° to the foliation. A later set of thicker (c. 50 cm wide) undeformed pegmatitic veins cut the intense, N–S, L–S fabric within the conglomerate (Fig. 4D). These late pegmatite veins contain large undeformed crystals of white mica and trend as vertical sheets generally sub parallel to the N–S lineation in the surrounding conglomerate.

3.1. Techniques of strain analysis

Conglomerates are commonly employed for strain analysis using the Rf/φ technique (Ramsay, 1967; Dunnet, 1969; Lisle, 1985). These procedures use the axial ratio (Rf) and orientation (φ) of clasts in the deformed rock as parameters to determine the strain. The present analysis uses the θ-curve method (Lisle, 1985) which is a development of the Rf/φ technique (Dunnet, 1969; Law, 1986; Yoshinori and Wallis, 2002). A major benefit of the θ-curve method is that it permits evaluation of appropriate errors for the strain estimates. For comparison, in addition to the θ-curve fitting method, the finite strain was also calculated using the harmonic mean. Though widely used, the Rf/φ technique has two main drawbacks:

1. The strain ratio recorded may tell nothing of the strain within the whole rock if there is a viscosity contrast between the deforming markers and the matrix (Freeman and Lisle, 1987).
2. There is no method to define outlying data, nor any method to quantify its effect on the analysis (Yoshinori and Wallis, 2002).

Hence, two additional methods were used to present a measure of the whole rock strain and to quantify outlying data. The Fry method is used to gauge the whole-rock strain (Fry, 1979). A regression method is also presented that provides a means of accommodating outliers within the data.

In all samples, the three ratios of the strain ellipsoid are assumed to lie within the foliation plane. In this study three reference planes orientated: (i) perpendicular to the foliation and containing the lineation, and (ii) perpendicular to both the lineation and foliation and (iii) the foliation plane containing the stretching lineation and the intermediate axis, have been used. These planes are assumed to be parallel to the *XZ*, *YZ* and *XY* principal planes of finite strain. The 3-D strain can be determined by combining the 2-D data from any two of these planes. This is an over determined system and thus can be used to evaluate internal consistency. Following normal convention, the symbols Ri, Rf, Rs are used to represent the aspect ratios of clasts in the unstrained and strained states and the aspect ratio of the strain ellipse, respectively. The value φ is the angle between the long axis of a clast in the deformed state and the trace of the foliation. Strain analysis was undertaken on 11 slices of conglomerate measuring more than 680 psammite clasts (Table 1).

This analysis provides direct evidence of the magnitude and strain ellipse orientation for $D2^M$ deformation within the Magerøy Nappe. Rf/φ analysis employed binary images produced from digital photographic images of polished rock slices. The binary images were created by tracing the boundaries of the clasts in a graphics program and saving the output in .BMP format. This resulted in superior definition of clast boundaries than fully automatic boundary definition within the measurement software. The .BMP files were analysed using Sicon image (e.g. Shaw et al., 1995), which automatically fitted ellipses to the traced clasts and determined lengths of the long and short axes, orientation of long axes relative to a reference line and the positions of the clast centres. The tabulated data were exported into

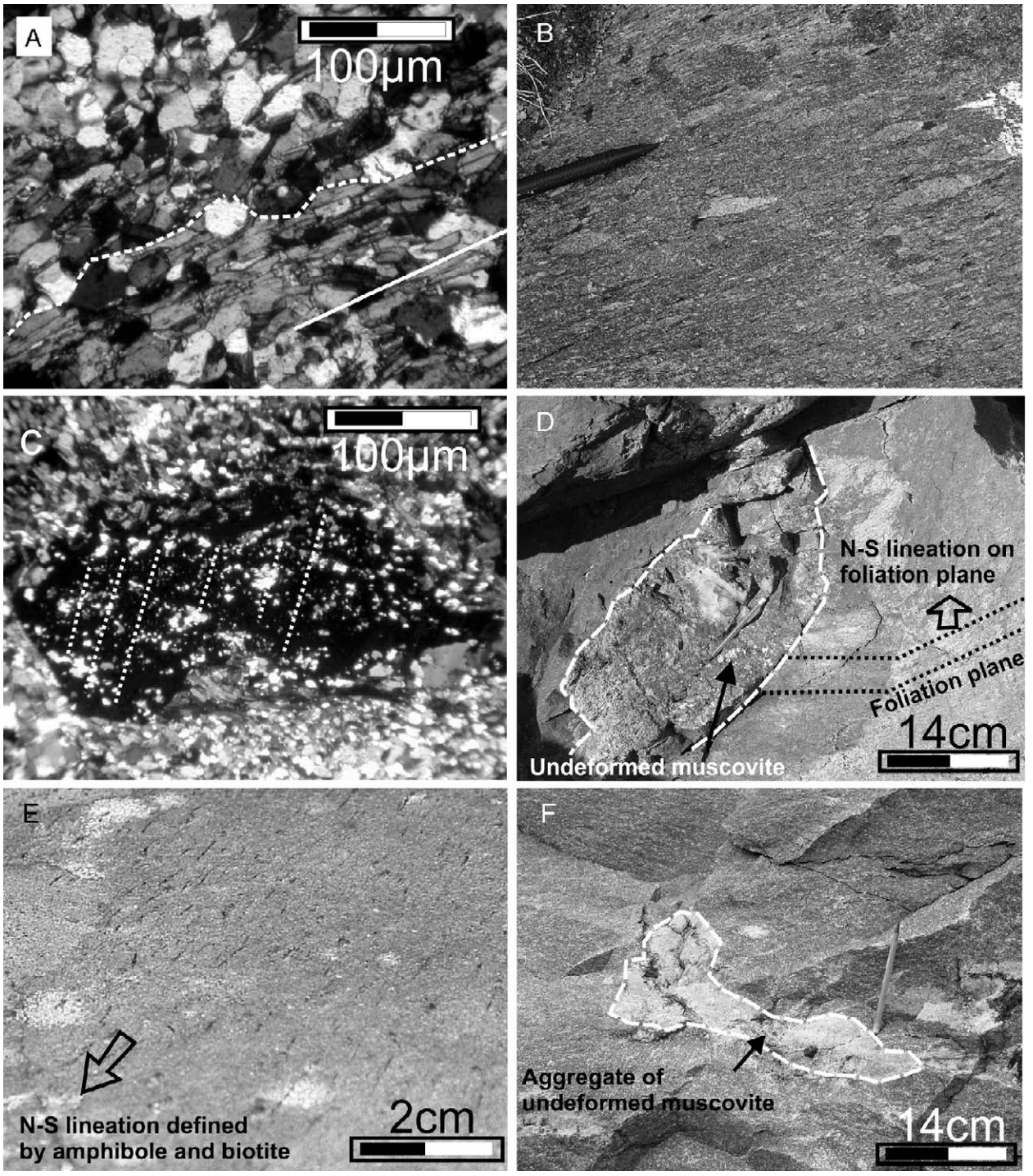

Fig. 4. (A) Photomicrograph of Hellefjord Schist conglomerate (CK060) showing the contact (white dashed line) between psammite clast (above) and matrix (below). Rugosity of the contact is interpreted as evidence of rheological similarity between the two. Biotite foliation is indicated by the solid white line; (B) conglomerate at base of Hellefjord Schist at Gamnes point, Sørøy, with light-coloured prolate psammite clasts used in the strain study, pen for scale; (C) photomicrograph of a thin section cut perpendicular to the foliation and parallel to the lineation in Hellefjord Schist conglomerate (CK060), showing garnet fractured and extended parallel to the intense N–S lineation; (D) undeformed granite pegmatite containing large undeformed muscovite crystals (labelled), from CK231 sample locality, cutting the N–S lineation in the Hellefjord Schist; (E) N–S mineral lineation defined by biotite and amphibole defined in typical pelitic lithology of the Hellefjord Schist, Bakfjord, Porsangerhalvøya; (F) weakly-deformed pegmatite cutting intensely deformed N–S lineation in the Bakfjord Granite (see Kirkland et al., 2005a). Note aggregate of undeformed muscovite (sample CK253) and biotite within the pegmatite.

Table 1
Summary of Rf/φ analysis showing the harmonic mean, the Rs value from the lowest χ^2 after Lisle (1985), the range of Rs at the 5% significance level, the arithmetic mean and weighted mean of Rs on each orientation of the finite ellipse

[70.6761807/23.2082587]						Range			
CK060	Plane	Number of clasts	Harmonic mean	Rs from lowest χ^2	χ^2	Lowest	Highest	Mean Rs from lowest χ^2	Weighted mean Rs (95% conf)
XY									
SLICE 1	*XY*	74	3.686	3.79	5.459	3.40	4.00	3.93	3.89±0.059
SLICE 2	*XY*	127	4.004	3.9	14.575	3.87	3.90		
SLICE 3	*XY*	54	4.023	4.1	7.481	4.00	4.80		
Total/average of hamonic mean		*255*	*3.904*						
XZ									
SLICE A	*XZ*	29	6.308	6	1.862	5.70	6.30	5.705	5.79±0.86
SLICE B	*XZ*	73	5.750	6.12	3.849	5.20	6.50		
SLICE C	*XZ*	64	5.213	5.6	3.813	5.10	6.20		
SLICE D	*XZ*	54	4.362	5.1	8.963	4.80	5.80		
Total/average of harmonic mean		*220*	*5.408*						
YZ									
SLICE 1 A	*YZ*	32	1.707	1.38	3.000	1.30	1.60	1.525	1.55±0.24
SLICE 2 B	*YZ*	61	1.745	1.4	3.426	1.40	1.60		
SLICE 3 C	*YZ*	82	1.745	1.68	*3.366*	1.50	1.70		
SLICE 4 D	*YZ*	31	1.913	1.64	0.452	1.50	2.00		
Toral/average of harmonic mean		*206*	*1.778*						
								Rxy measured / Rxy computed xy/(xz/yz)=1.05	

statistical programs to analyse the data. The use of digital images for measurements permits a high degree of accuracy by enabling magnification to precisely determine grain boundaries (Fig. 5). Rf/φ analysis was performed using the Excel spreadsheet macro of Chew (2003) (see Table 1). Fry analysis using R. Holcome's Fry Plot programme was used to gauge the bulk strain and determine if it was substantially different from the strain recorded in the clasts (Treagus and Treagus, 2002). The measured two dimensions of the finite strain ellipse were

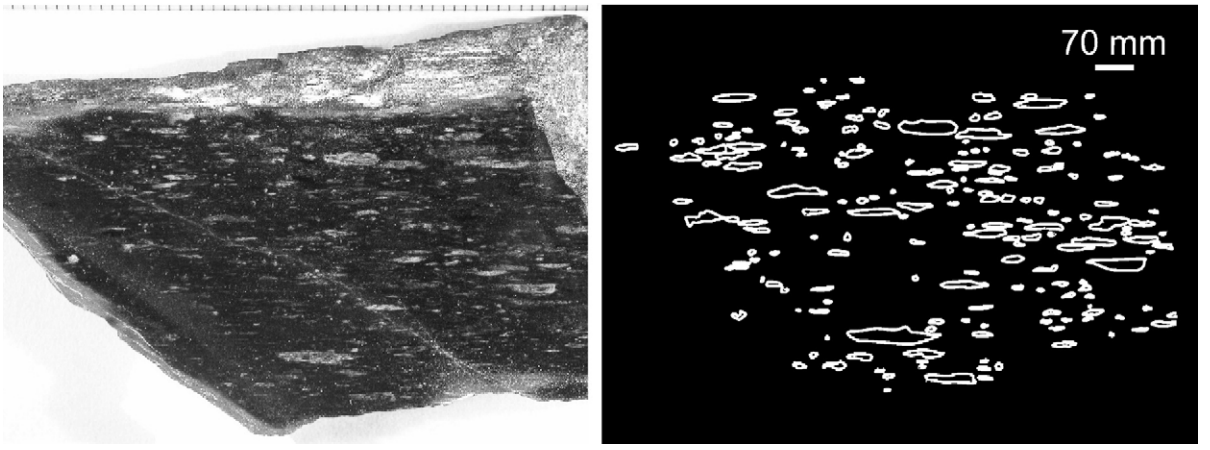

Fig. 5. Left, slice 1 showing the *X*–*Y* plane of the conglomerate sample CK060. Right, the corresponding digitized binary colour image highlighting clasts used in Rf/φ analysis.

also used to calculate linear regressions, which allowed calculation of the one unmeasured direction within a slice along a principal axis of the strain ellipsoid.

3.2. Interpretation of Rf/φ data

Details on the Rf/φ technique are presented in Appendix B. All data pass the symmetry and θ distribution tests (Lisle, 1985, Table 1). Both tests evaluate whether a primary fabric is present in the sample. Critical values for I_{sym} and χ^2 tests depend on the number of clasts measured and the measured strain and are given in Lisle (1985). The Rf/φ plots are bilaterally symmetric for all slices of the three orientations. The data show that the mean orientation of the long axes of the clasts lies parallel to the trace of the foliation and there is no obvious asymmetry (Fig. 6). Application of the symmetry test shows that the data are statistically symmetrical. As no oblique initial fabric occurs in the clasts an initial random distribution may be assumed.

By comparing the data to various θ-curves corresponding to different values of Rf we determine the appropriate range of strain ratios (Fig. 6). The data are fitted to the curve using a χ^2 test (Lisle, 1985). Any estimates of strain that implied a probability of less than 0.05 of actually observing the recorded data are rejected (Table 1). The results for Rs are 3.93, 5.71 and 1.53 for the *XY*, *XZ* and *YZ* planes of finite strain ellipsoid, respectively (Table 1). All slices show prolate geometries with the maximum extension direction within the foliation plane and orientated N–S.

Dependant on the viscosity contrast between clast and matrix, Rf/φ analysis performed on the clasts fraction may not provide a measure of the whole-rock strain. The clasts represent approximately 15% of the rock volume, and thus their Rf/φ analyses may only elucidate part of the strain in the conglomerate. However field and petrographic evidence suggests that there is little competence contrast between the psammitic matrix and psammite clasts, as no curvature of matrix foliation is seen around clasts. The accuracy of this Rf/φ triple strain measure is assessed later, using the Fry point-to-point method to corroborate the value recorded in the rock matrix with that of the clast. Using the mean Rs value at the lowest value of χ^2 for the strain on *XZ* and *YZ* sections gives a triple strain ratio for the clasts of 4:1.5:1. Using the harmonic mean does not result in markedly different results as would be expected in this high strain regime (Borradaile and Johnson, 1973; Lisle, 1977; Table 1). Assuming no volume change these values convert to bulk stretches of $X=2.17$, $Y=0.84$ and $Z=0.55$, lying to the prolate side of plane strain orientated in an N–S direction. If the triple strain is calculated from the *XY* and *YZ* sections, bulk stretches of $X=2.85$, $Y=0.73$ and $Z=0.48$ are produced. Thus the psammite clasts suffered a shortening of c. 50% assuming no volume loss.

Determining volume loss during deformation within the conglomerate is difficult. There is no geological evidence in the form of intrusions or other features that suggest that a significant volume of material was added, at this locality, during the $D2^M$ deformation. After deformation, however, pegmatitic material was added in the form of undeformed veins. Microprobe analyses across the biotite clots within the conglomerate show negligible differences in major element composition (Kirkland et al., 2006b). These data suggest that little local volume or areal change by diffusion of mobile elements occurred. However, some degree of recrystallization is suggested in a few of the psammitic clasts (<3%) which display grain size reduction along their grain margins. The thickness of these boundaries is not proportional to clast size.

In strongly recrystallized fabrics, grain/clast shapes must be interpreted with caution, as they will preserve information on the last increment of deformation, not necessarily the finite strain. If it is assumed that the recrystallization boundaries were, at a maximum, 50% greater in size, which is probably an over estimation of the degree of grain size reduction, this would correspond to a volume loss of 0.1% based on the smallest clast size showing evidence of recrystallization. The error, from this hypothetical degree of recrystallization, corresponds to an insignificant difference in triple strain ratio. It is concluded that the degree of recrystallization of the psammite clasts has a negligible bearing on the measurement of the finite strain in this sample. A volume loss of 5%, which is considerably greater than that undergone by the psammite clasts, would result in approximately only 1% difference in maximum shortening recorded. Moreover, because the strain measurements were made at the millimetre (Rf/φ analysis) and tens of centimetre scales (Fry analysis) and both studies yielded almost identical results (see below), it is likely that the scale at which strain was measured greatly exceeds the length scale of any volume change within the conglomerate.

3.3. Clast strain and bulk rock strain

The Rf/φ analysis elucidates the clast strain within the conglomerate, but, may not yield a useful measure of the whole rock strain. Thus we have applied an automated method of Fry analysis (outlined above) on the same rock slices that were used in Rf/φ analysis. Fry analysis is based on the assumption that the clasts and, by

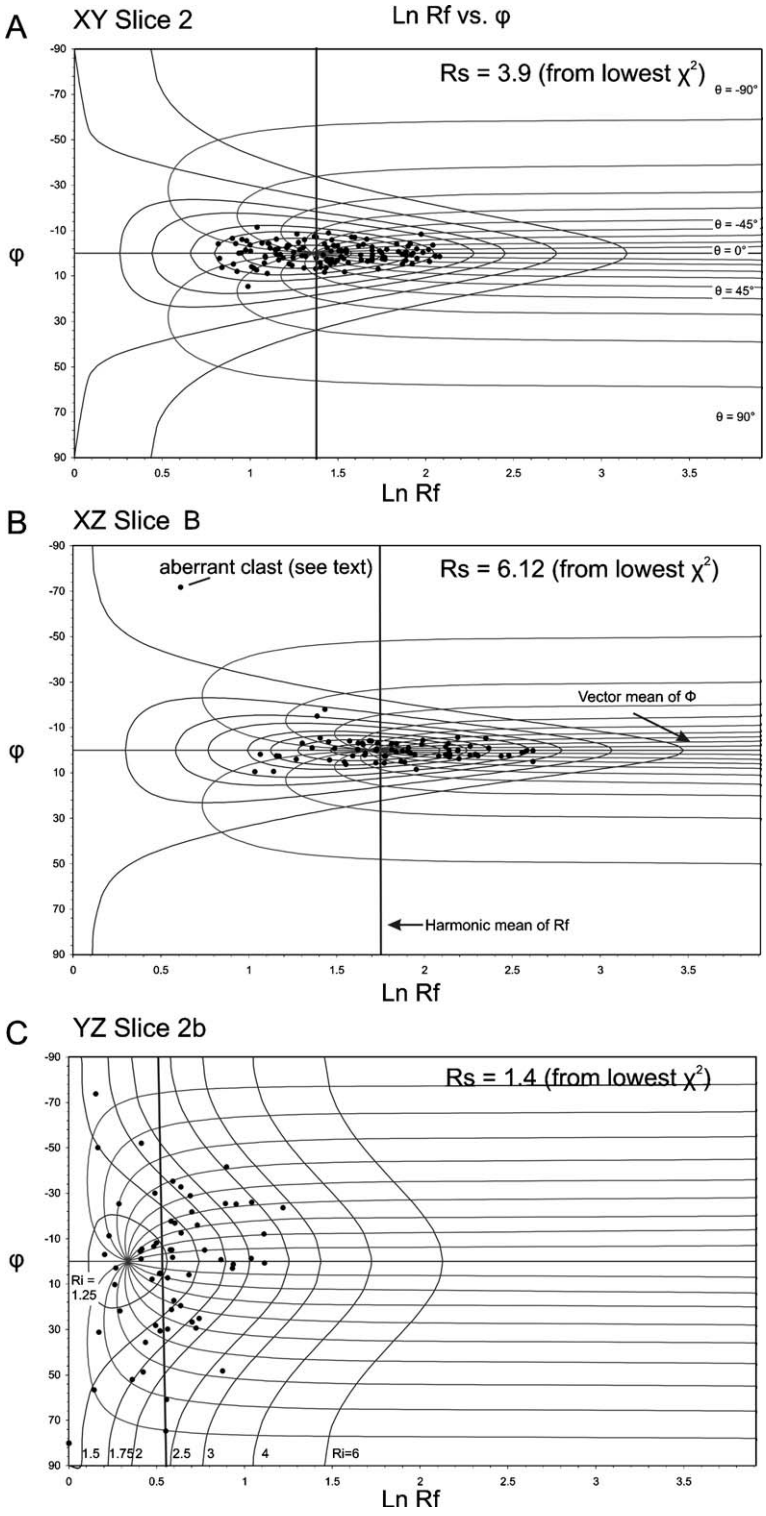

Fig. 6. Selected Rf/φ plots produced using the Excel™ macro of Chew (2003). Contours of *Ri* (1.5, 1.75, 2.0, 2.5, 3, 4, 6) and θ (with the 90°, 45°, 0°, −45° and −90° curves labelled) superimposed on the original data for strain ratios, Rs = 3.9 for the *XY* surface (A), = 6.12 for *XZ* (B) and = 1.4 for *YZ* (C). For a good fit, 5% of the data should lie within any two adjacent curves where the left and right hand sides are distinguished.

inference, their centres were originally in an anti-clustered distribution. A strong halo of points was not displayed in any of the rock sections analysed. Thus, following the method used by Treagus and Treagus (2002), a best fit ellipse was sought that had its long axis parallel to the extension axis and that maximized the number of innermost points on the ellipse trace (Fig. 7). In some cases no clear vacancy was present and hence no meaningful ellipse could be produced. However, several rock slices in each of the three orientations produced satisfactory vacancies in which an ellipse could be fitted. The best-defined ellipse was chosen in each case as the measure of the ellipse ratio within that strain ellipse orientation. In each case these are orientated approximately parallel to the foliation and *X* direction. The method yields a triple strain ratio of 2.51:0.78:0.51 from the *XY XZ* slices and 2.65:0.82:0.46 from the *XY YZ* slices corresponding to shortening of approximately 50%. These values are not significantly different from the values of the triple strain ratio of the psammite clasts.

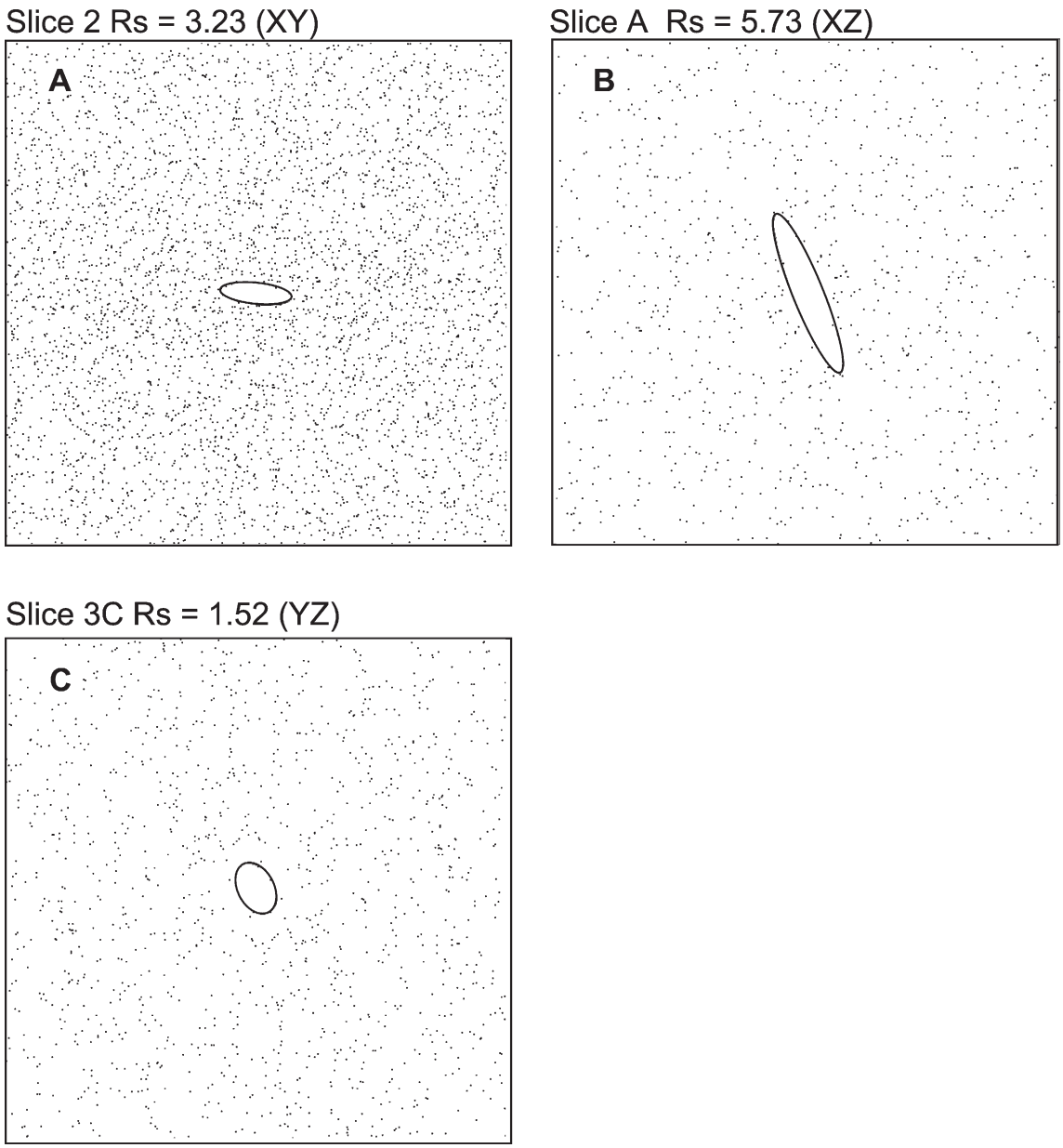

Fig. 7. Fry analyses of conglomerate (CK060). (A) Analysis of slice 2, *XY* section; (B) slice A, *XZ* section; (C) slice 3C, *YZ* section. The best-fit strain ellipses are outlined on each figure, and their Rs values are shown. See also Table 2.

This confirms the field observation of clasts appearing to deform in a similar manner to the matrix. This is expected as both clasts and matrix are of a similar lithology, namely psammitic clasts supported within a psammite matrix.

3.4. Calculated clast triple lengths

In order to assess the effect of outliers within the data least squares regression analysis has been performed on each set of clast measurements. Regression analysis is used to investigate and model the relationship between a response variable and a predictor, in this case the response and predictors being clast lengths in various orientations of the finite ellipse. Each orientation of slice enables measurement of two out of the full three ratios of the finite ellipse defined by the deformed clast. Thus within one orientation of slice, (*XY*) for example, two regressions are possible— one to find *X* from *Y* and its inverse to find *Y* from *X* (Fig. 8). Hence, because data are available from each orientation of the strain ellipse, each clast length can be found from two regressions, i.e. *X* predicted from *Y* and *X* predicted from *Z*. Some simplifying assumptions distinct to those used in Rf/φ analysis are necessary for the regression equation to be used for an estimate of strain. A linear relationship between clast length for all orientations is assumed, i.e. the *X* direction is assumed to be linearly related to the *Y* and *Z* directions. As a clast's maximum dimension increases, so do its intermediate and minimum lengths. The slope of the best-fit straight line through the origin on a plot of minor axis versus major axis gives the mean value of strain on that section of the finite strain ellipse (Ramsay and Huber, 1983, Fig. 8). However, neither assessment of outliers nor the incorporation of data from other sections of the strain ellipse can be considered by simply taking the best-fit slope. Using the straight-line equation from least squares regression allows the validity of the slope to be assessed graphically when used with data from one of the other two dimensions of the finite strain ellipse (Figs. 8 and 9).

4. Strain analysis results

Eight linear regressions were performed on the clast lengths measured (Fig. 8). The *R* and adjusted *R* values represent the proportion of variation in the response data explained by the predictors. For the *XY* slice this is 70.6%; the *XZ* slice 52.1%; and the *YZ* slice 73.5%. For the majority of length data more than 70% of the clast length variation in one axis can be explained by the length variation on another axis. The lower value of 52.1% prediction of *X* from *Z* and *vice versa* reflects the effect of predicting the most dissimilar orientations, that is using the longest axis to predict the shortest and *vice versa*, hence the dispersion is greater from a perfect linear relationship. Making the simplifying assumptions described above, regressions were used to calculate the length of the missing dimension within the dataset of measured clast dimensions. These data were plotted on a Flinn graph to assess the strain (Fig. 9), contouring the density of points using the Arcview™ compute density function as described by Mitchell (1999). This illustrates the number of data points per given area of strain space. Each missing axis is described by two linear regression equations. Data from each regression equation are plotted independently and assessed before the mean of the density of both regressions is plotted (Fig. 9). The mean density of both regressions is considered to represent the best estimate of the strain by this method. The maximum density clusters of the mean measurements on the *XZ* and *XY* slices correspond well to the mean strain value from the Rf/φ analysis, using the *XY YZ* sections (Fig. 9). In all cases the data show greater dispersion along the *XY* axis of the Flinn graph corresponding to the measurement on the *X* axis showing the greatest standard deviation (i.e. *X*, 3.9). Measurement of the *Y* and *Z* clast lengths show increasingly smaller standard deviations (*Y*, 1.7; *X*, 0.7).

The *YZ* slice mean density plot has its maximum density contour at higher strain than that observed from Rf/φ analysis and also, critically as an independent measure of data consistency, different from the maximum contours of the other mean density plots (Fig. 9). This may relate to a bias in the construction of the initial binary image and provides a method to evaluate the presence of outliers in the data. Looking at the individual regressions that make up the mean density plot, it is apparent that the *XY* regression is over-estimating the value of *X*. Considering the individual measurements used to derive the regression, one pronounced outlier is found, the largest value from slice 3 along the *XY* axis of the finite strain ellipse (Fig. 8). Evaluating this outlier "clast" reveals that it represents up to seven different individual clasts in close proximity yielding the artificial impression of a singular large clast. Excluding this one "clast" out of the total of 255 included in the least squares regression yields a more satisfactory line, whose mean density plot is closer to that recorded on the other axis of the ellipse (Fig. 9). It yields a maximum contour of mean density close to the mean strain value from Rf/φ analysis (Fig. 9). Omitting this one clast also affects the regression equation produced for the *XZ* slice as *Y* is predicted from *X* also. The effect from the modification

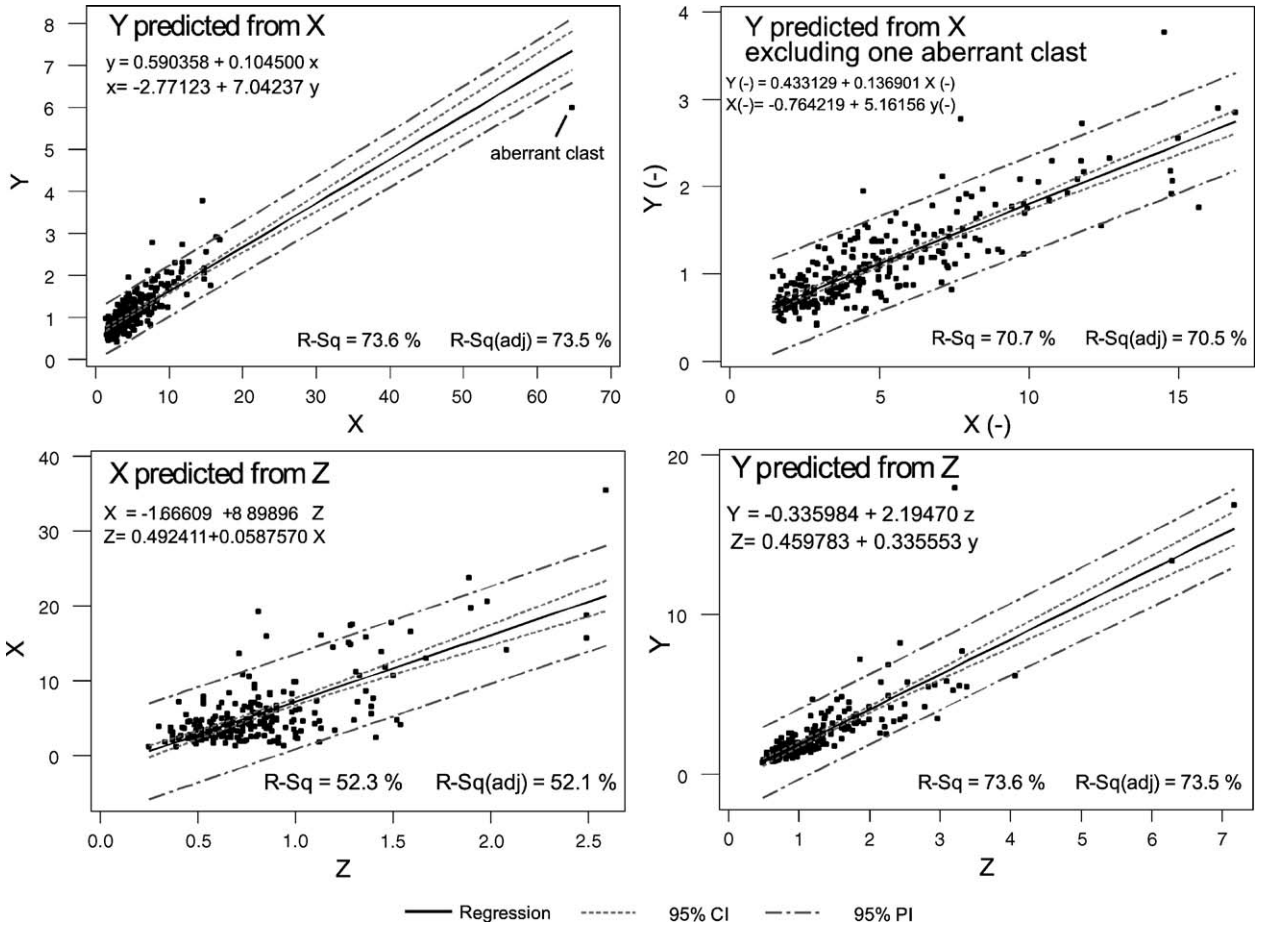

Fig. 8. Linear regressions with 95% confidence bands (Cl) of the long, intermediate and short axes of psammite clasts in sample CK060. In each case the strain ratio in two dimensions is given by the slope of the line. 95% prediction bands (Pl) are also shown.

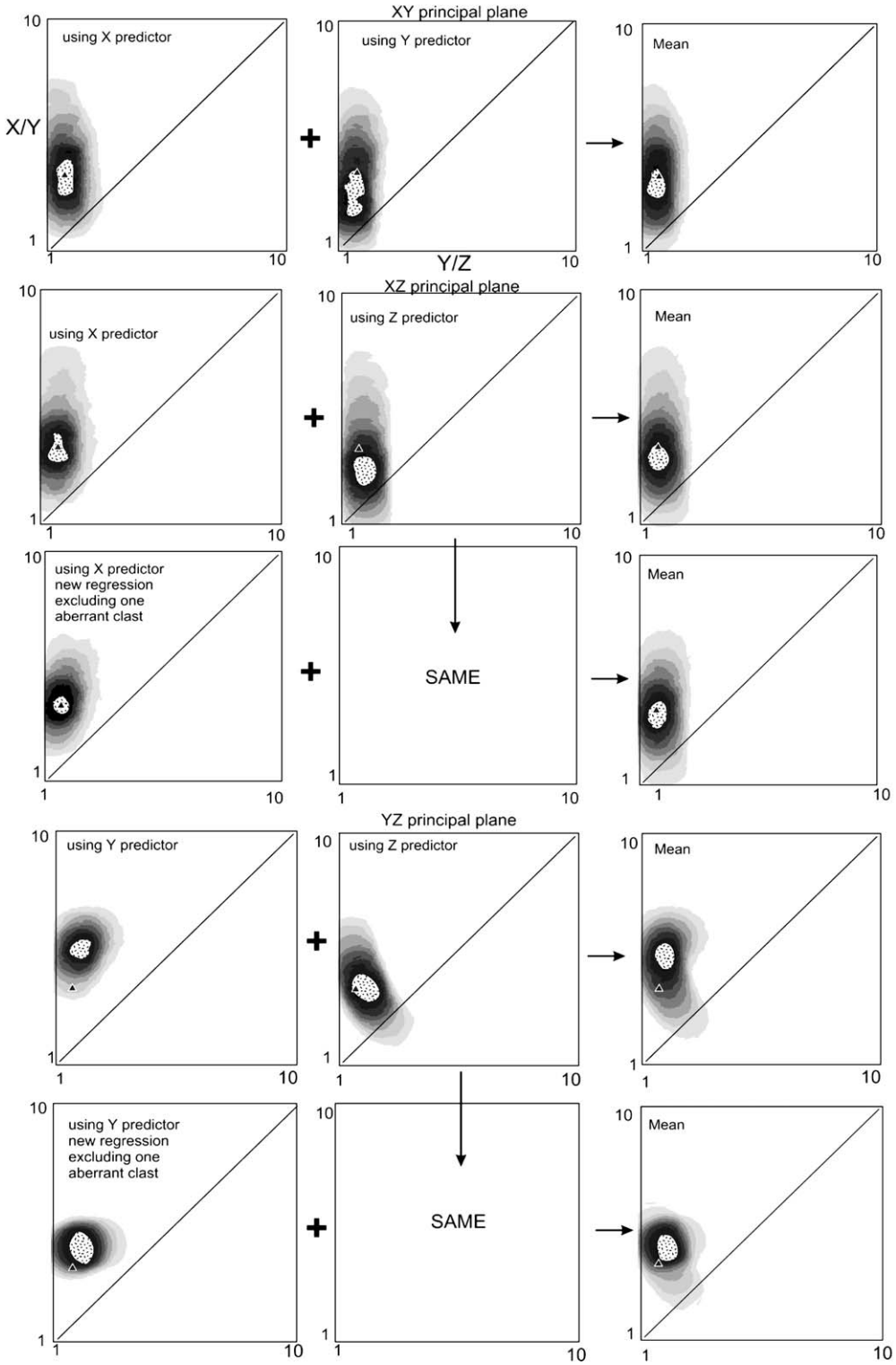

Fig. 9. Contour density Flinn plots produced from the linear regression equations (based on all measured clasts, see Fig. 8). The regression equations are used to determine the length of the one missing clast axis. Each missing clast axis can be found from two linear regression equations. Both equations for each axis are plotted independently and the mean of both is shown on the right. The regression equation excluding the aberrant "clast" yields a measure of strain closer to the Rf/φ analysis. Contour intervals are in increments of 1/8th of the maximum density per unit of strain space.

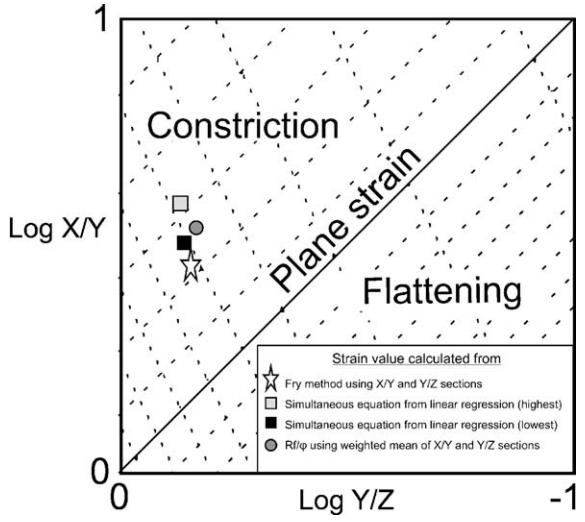

Fig. 10. Logarithmic Flinn diagram showing the strain values calculated from each of the methods of strain analysis (Fry, Rf/φ, combined linear regressions). All values lie in the constriction field and show little variation.

of its regression equation on the position of its highest density spot is insignificant (Fig. 9). The regression omitting the single outlier produces a mean density plot for the *YZ* slice that is closer to the mean value from Rf/φ analysis, although it still over-estimates the strain magnitude by a small margin. Omission of the composite "clast" from the *XY* slice 3 (Table 1) has a negligible effect on the Rf/φ analysis, lowering the χ^2 value marginally to 5.6, but not affecting the value of Rs from the lowest χ^2. However in a situation where more aberrant clasts were measured, their identification and omission using this method could substantially improve the Rf/φ measure of strain.

By simply taking the slope of the regression line, an estimate of the strain is possible (Ramsay and Huber, 1983; Fig. 8). However, it must be remembered that the line can be greatly influenced by the presence of outliers and in addition the method uses information from two dimensions. The slope values for the *XY* plane are 7.04, *YZ* 2.19 and *XZ* 8.90, corresponding to a triple strain ratio (assuming no volume change) of 3.3:0.81:0.37 using the *X*/*Z* and *Y*/*Z* sections (Fig. 8). Using the *X*/*Y* section along with either of the remaining two, results in an over estimation of the strain for the reasons discussed above. Using the improved regression (i.e. omitting the aberrant clast), a value consistent with that calculated from the other sections is produced (i.e. 3.88:0.74:0.34; *X*/*Y* and *Y*/*Z*; Fig. 8). No indication of multiple slopes such as that caused by ductility contrasts in the clasts is observed.

Three regressions can be used to form a simultaneous equation which can be solved for values of *X*, *Y* and *Z*. Out of the total of six linear regressions (i.e. excluding the two with the aberrant "clast"), two for each axis of the finite ellipse, the regression produced from the longest available orientation of finite ellipse is first used as a predictor (i.e. *X* from *Y*, *Y* from *X* and *Z* from *X*). The calculation is then repeated using the shortest orientation of finite strain ellipse as a predictor (i.e. *X* from *Z*, *Y* from *Z* and *Z* from *Y*), yielding a range in which the actual strain lies (Table 1; Fig. 10).

Results for the simultaneous equation using the longest available axis yields: $-X=5.015$, $Y=1.120$, $Z=0.787$ (*R* strain aspect = 4.9) and; $X=2.426$, $Y=0.673$, $Z=0.460$ (*R* strain aspect = 4.1) from the shortest available axis.

On a Flinn diagram (Fig. 10), the aspect ratios of the strain ellipsoid determined from measurement of the clasts using all three of the above methods shows a clear departure from plane strain. This difference from plane strain can be expressed using the parameter $K = \mathrm{Rs}(XY) - 1/\mathrm{Rs}(YZ) - 1$ also $\mathrm{Rs}(XY) = \mathrm{Rs}(XZ)/\mathrm{Rs}(YZ)$ (Table 2). On a Flinn diagram, plane strain deformations plot along a line inclined at 45° and have a *K* value of 1. This line separates constrictional strain where at least two axes of the principle ellipse are contracting ($k>1$) and flattening deformation where at least two axes are undergoing extension ($k<1$). The results for *K* of the four different determinations of strain using the *R xy* and *R yz* sections are: $k=5.25$ (weighted mean of θ-curve method), $k=4.29$ (Fry method), $k=3.72$ (harmonic mean) and $k=8.29$–

Table 2
List of Rs values from the various methods used from all three axes of the strain ellipse. *XY* and *YZ* planes used in all calculations. Values of *X*, *Y* and *Z* are calculated assuming constant volume

Method		R xy	R xz	R yz	R xz meas / R xz comp	X	Y	Z	K	L	N
Rf/φ		3.89	5.79	1.55	0.96	2.86	0.74	0.47	5.58	−0.53	1.32
Fry		3.23	5.73	1.52	1.17	2.51	0.78	0.51	4.29	−0.47	1.17
Harmonic mean		3.90	5.41	1.78	0.78	3.00	0.77	0.43	3.72	−0.41	1.41
Combined linear regression	*using longest avaliable axis*	4.48	6.37	1.42	*1.00*	3.05	0.68	0.48	8.29	−0.62	1.39
	using shortest available axis	3.60	5.28	1.46	*1.00*	2.66	0.74	0.51	5.65	−0.54	1.23

K is the logarithmic *K*-value after Flinn (1962) adapted by Ramsay (1967). *L* is Lode's shape parameter (Lode, 1926). *N* is Nadai's strain parameter (Nadai, 1963). The ratio of the measured to computed values of *R xz* is used to assess the internal consistency of the data.

5.65 (linear regression combined using simultaneous equations, Fig. 10). These results show some variation, all indicating that the strain lies in the constriction field but that extension is occurring in a N–S orientation.

Geometric analyses of thrust systems commonly assume that strain is essentially two-dimensional (plane strain— no movement of material across the transport plane) in which the linear element of the grain shape fabric indicates the transport direction. Numerous studies have shown that plane strain may be considerably less common than typically envisaged within thrust belts (Northrup and Burchfiel, 1996; Neves et al., 2005). Top-to-the-east kinematics are preserved within the Hellefjord Schist, and indeed throughout the Magerøy Nappe and KNC (Gayer et al., 1987). In the situation examined within the conglomerate at the base of the Hellefjord Schist, prolate strain has been imposed on the rocks and is responsible for an intense N–S lineated fabric lying at a high angle to the top-to-the-east transport direction. Intense N–S lineated fabrics are also found elsewhere within the Hellefjord Schist (Kirkland et al., 2005a Fig. 4.E). The strain results in this paper indicate c. 50% horizontal shortening parallel to the thrusting direction and c. 200% extension along the orogenic strike with c. 30% vertical shortening. These strain measurements are from near the base of the Magerøy Nappe and likely reflect a maximum value within this nappe. However, a similar deformation style has been imposed regionally as indicated by the pervasive N–S fabric throughout the tectonostratigraphy.

Lode's (1926) shape parameter (L) expresses the prolate nature of all the strain measurements with values between −0.41 and −0.62. Nadai's (1963) octahedral shear strain parameter (N) is used as an expression of strain magnitude and shows values between 1.17 and 1.39 (Table 2). Values of octahedral shear strain from the Moine Thrust using grain shape fabrics in mylonitic quartzites show values of 1.10–1.47 for relict footwall grains (Strine, 2003). The strain measurements presented here appear reasonable for the strong L–S tectonite conglomerate unit in the Hellefjord Schist. Within fold nappes, strain types and magnitudes can vary (Ramsay and Huber, 1983; Seno et al., 1998). Nonetheless, the consistency of the N–S linear fabric and its timing of development (see below) suggests the same formation mechanism throughout all nappes.

5. Ar–Ar dating, constraint on the age of Scandian fabrics

In order to provide temporal constraint on the $D2^M$ fabric investigated in the strain analysis, the age of undeformed white mica grains within cross-cutting granitic pegmatites have been determined by Ar–Ar furnace heating experiments. Muscovites from a psammitic unit in the Hellefjord Schist at Bakfjord and the Storelv Schist in the Havvatnet Imbricate Stack were also investigated. A single sample of biotite from the c. 438 Ma Engesfjellet Granite on Sørøy was also analysed. The analytical procedure is given in Appendix C. All errors reported in the text are at the 2σ level unless otherwise stated and include the uncertainty in the J value (1%).

5.1. CK231

Undeformed large white mica crystals, up to 50 mm across, were analysed from an undeformed granitic pegmatite that cuts the intense L–S fabric within the conglomerate unit used in the strain study (Fig. 4D). Ar–Ar furnace heating data are presented in Fig. 11A and in Table 3. Sample CK231 displays a relatively concordant age spectrum in which apparent ages rapidly increase in the initial low-temperature, low gas volume steps. Most of the data from intermediate- and high-temperature increments (938–1091 °C) record consistent ages. This stable portion of the release spectrum yielded a weighted mean age of 418±6 Ma corresponding to 82.3% of the gas released; this age is used in the subsequent discussion. An inverse isochron could not be calculated due to the clustering of data and the small analytical errors.

5.2. CK224

Sample CK224 (Fig. 1) is from a boudinaged pegmatite intruding parallel to the foliation within the enclosing Hellefjord Schist at Hellefjord, 6 km NE of sample CK231. The pegmatite is itself unfoliated and contains large crystals up to several cm of both tourmaline and white mica. Ar–Ar analyses of white mica grains define a gentle saddle-shaped spectrum (Table 3). However >85% of the gas evolved records a weighted mean age of 415±6 Ma (Fig. 11B). Unfortunately due to rapid degassing at intermediate temperatures there are only two near-plateau steps. Nevertheless, an inverse isochron of these yields a $^{40}Ar/^{36}Ar$ intercept of 294±4, identical within error to the atmospheric value (Fig. 11B).

5.3. CK206

This sample consists of porphyroblastic muscovite from a foliated psammite (CK206) within the Hellefjord Schist close to the contact with the c. 438 Ma Bakfjord Granite (Kirkland et al., 2005a). The furnace release

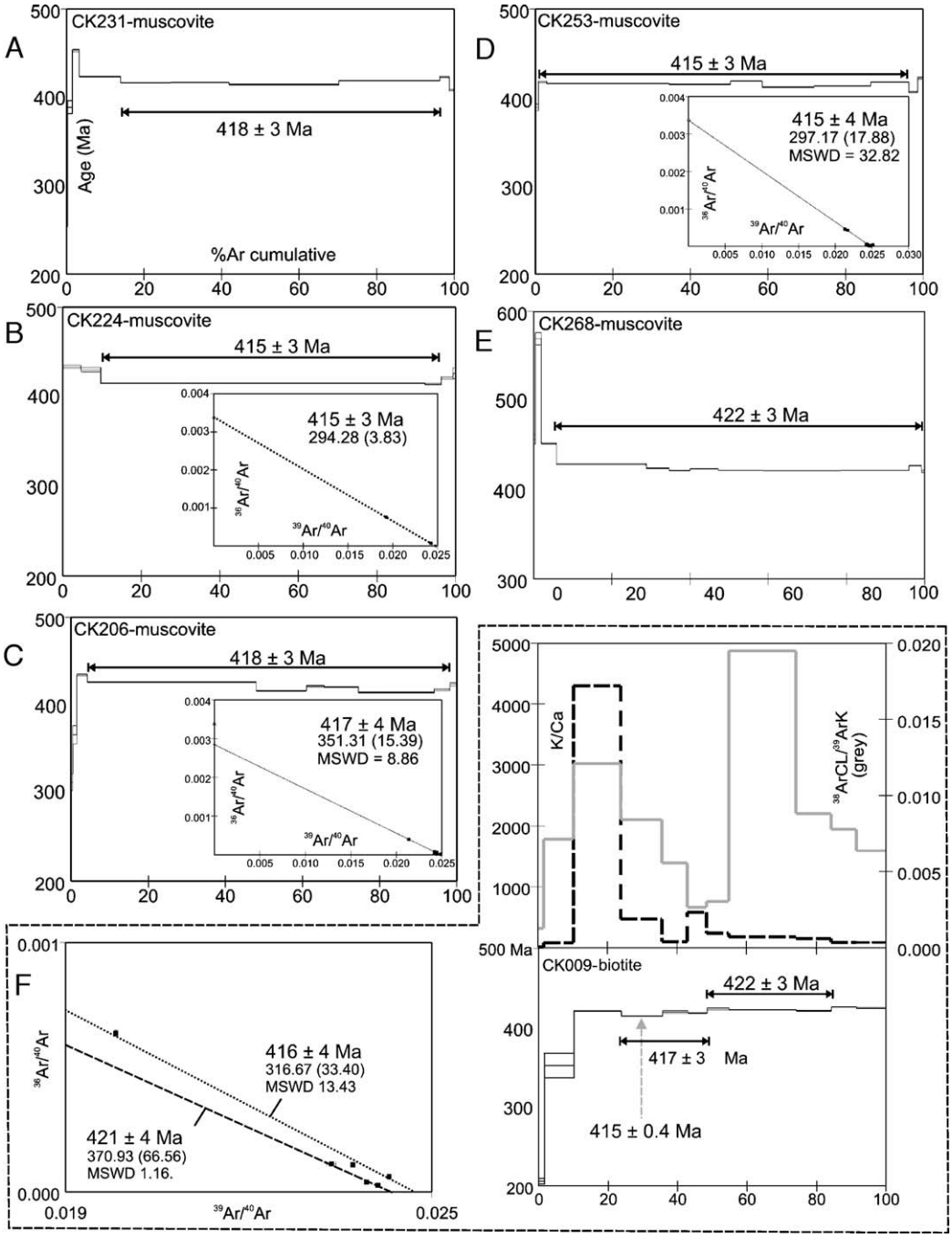

Fig. 11. $^{40}Ar/^{39}Ar$ resistance-furnace step-heating release spectra (A–F) for mica samples showing weighted mean ages calculated over the indicated portions of the spectra. (B) and (D) inverse isochrons for muscovite from CK224 and CK 253, that overlap with the weighted mean age within uncertainty and whose upper intercepts indicate an atmospheric trapped argon component; (C) inverse isochron of muscovite from CK206, that overlaps with the weighted mean age but with an intercept consistent with a non-atmospheric trapped argon component. The inverse isochron age is preferred; (F) biotite from CK009 displays two trapped argon components. The younger inverse isochron, which is interpreted as a maximum age for the cooling of biotite in this rock, has a poor fit to the data but intercepts at the atmospheric value. The intercept of the older inverse isochron indicates a non-atmospheric component. The two populations are also evident in the K/Ca and $^{38}ArCl/^{39}ArK$ plots. All errors are 1σ.

Table 3
Ar–Ar isotopic analyses for each temperature step together with the cumulative percentage of ^{39}Ar released ($F^{39}Ar$), the *J* value for each sample and calculated ages with 1σ errors

CK268 muscovite		*J=.0064350 (70.6760252/23.2085806)*								
Temp (°C)	$^{40}Ar/^{39}Ar$	$^{38}Ar/^{39}Ar$	$^{37}Ar/^{39}Ar$	$^{36}Ar/^{39}Ar$	^{39}Ar (mol)$\times 10^{-15}$	$F^{39}Ar$	$\%^{40}Ar^*$	$^{40}Ar^*/^{39}Ar_K$	Age (Ma)	$\pm 1\sigma$
482	221.369	0.024	1.868	664.637	0.09	0.33	11.4	25.14	270.7	16.9
613	163.514	0.002	0.036	426.89	0.34	1.54	22.8	37.35	388.8	7.3
694	68.59	0.006	0.033	82.048	0.50	3.31	64.6	44.33	453.0	1.5
781	48.252	0.003	0.028	24.185	2.99	13.94	85.2	41.09	423.5	0.5
938	40.986	0.001	0	2.136	3.64	26.89	98.4	40.34	416.5	0.3
985	40.732	0.003	0	1.122	4.23	41.94	99.1	40.38	417.0	0.3
1034	40.237	0	0.012	0.319	7.96	70.26	99.7	40.12	414.6	0.6
1091	40.675	0.001	0	0.234	7.31	96.27	99.8	40.59	418.9	0.3
1136	41.578	0.002	0.205	1.768	0.69	98.73	98.8	41.06	423.2	0.9
1181	40.605	0	0.375	3.98	0.36	100	97.2	39.45	408.4	1.0
CK224 muscovite		*J=.0064090 (70.7173097/23.3026403)*								
Temp (°C)	$^{40}Ar/^{39}Ar$	$^{38}Ar/^{39}Ar$	$^{37}Ar/^{39}Ar$	$^{36}Ar/^{39}Ar$	^{39}Ar (mol)$\times 10^{-16}$	$F^{39}Ar$	$\%^{40}Ar^*$	$^{40}Ar^*/^{39}Ar_K$	Age (Ma)	$\pm 1\sigma$
702	56.641	0.017	0.004	48.166	5.38	4.66	74.8	42.39	433.8	1.7
799	43.224	0.001	0.003	4.087	5.87	9.74	97.2	42.00	430.3	2.3
916	41.259	0.002	0	3.159	95.30	92.23	97.7	40.31	414.8	0.1
950	51.846	0.004	0.048	39.155	4.74	96.34	77.7	40.26	414.4	1.0
984	50.349	0	0.005	31.648	3.49	99.36	81.4	40.98	420.9	1.5
1187	54.733	0.013	0.026	44.504	0.74	100	75.9	41.57	426.3	6.1
CK206 muscovite		*J=.0064600 (70.8494031/24.6314979)*								
Temp (°C)	$^{40}Ar/^{39}Ar$	$^{38}Ar/^{39}Ar$	$^{37}Ar/^{39}Ar$	$^{36}Ar/^{39}Ar$	^{39}Ar (mol)$\times 10^{-16}$	$F^{39}Ar$	$\%^{40}Ar^*$	$^{40}Ar^*/^{39}Ar_K$	Age (Ma)	$\pm 1\ \sigma$
498	63.483	0.003	0	115.748	0.55	0.49	46.1	29.26	312.5	9.5
614	192.974	0.028	0	535.08	1.16	1.53	18.1	34.84	366.4	10.4
701	46.699	0	0	15.46	3.07	4.29	90.2	42.11	434.3	1.1
822	46.784	0.003	0	18.676	48.70	48.03	88.2	41.25	426.4	0.5
905	40.88	0.002	0.037	2.331	14.50	61.04	98.3	40.18	416.5	0.5
970	41.363	0	0	2.108	5.11	65.62	98.4	40.72	421.5	1.1
1036	40.884	0.001	0	0.789	9.92	74.53	99.4	40.63	420.7	0.7
1110	40.157	0	0	0.627	21.90	94.17	99.5	39.95	414.4	0.8
1170	41.355	0	0	3.458	4.53	98.23	97.5	40.31	417.8	1.1
1247	43.933	0.007	0.449	10.189	1.97	100	93.2	40.95	423.7	2.0
CK253 muscovite		*J=.0064220 (70.8630878/24.6893102)*								
Temp (°C)	$^{40}Ar/^{39}Ar$	$^{38}Ar/^{39}Ar$	$^{37}Ar/^{39}Ar$	$^{36}Ar/^{39}Ar$	^{39}Ar (mol)$\times 10^{-16}$	$F^{39}Ar$	$\%^{40}Ar^*$	$^{40}Ar^*/^{39}Ar_K$	Age (Ma)	$\pm 1\sigma$
482	76.913	0.019	0.431	145.338	0.39	0.14	44.2	33.99	356.4	12.0
614	178.774	0.018	0.219	478.357	1.92	0.82	20.9	37.42	388.8	4.0
701	46.904	0.001	0.084	21.566	5.99	2.96	86.4	40.52	417.5	1.0
779	41.049	0.002	0.002	2.359	88.40	34.47	98.3	40.33	415.8	0.5
885	46.1	0.012	0	19.821	44.40	50.31	87.3	40.22	414.8	0.4
939	41.252	0.001	0.029	2.096	22.90	58.47	98.5	40.62	418.4	0.4
999	40.236	0.005	0.009	1.118	37.60	71.9	99.1	39.89	411.7	0.6
1041	40.228	0.005	0.021	0.561	41.00	86.53	99.5	40.05	413.1	0.4
1086	40.688	0.004	0.008	0.565	27.70	96.4	99.5	40.50	417.3	0.3
1140	39.772	0.006	0.198	1.659	6.19	98.61	98.8	39.28	406.1	0.9
1184	41.787	0.007	0.444	2.889	3.90	100	98.0	40.96	421.6	1.6
CK268 muscovite		*J=.0064470 (70.5506909/24.1126245)*								
Temp (°C)	$^{40}Ar/^{39}Ar$	$^{38}Ar/^{39}Ar$	$^{37}Ar/^{39}Ar$	$^{36}Ar/^{39}Ar$	^{39}Ar (mol)$\times 10^{-15}$	$F^{39}Ar$	$\%^{40}Ar^*$	$^{40}Ar^*/^{39}Ar_K$	Age (Ma)	$\pm 1\sigma$
500	59.304	0.043	0.321	49.757	0.23	0.45	75.2	44.62	456.4	5.5
610	94.475	0.048	0.088	125.031	0.80	1.99	60.9	57.52	569.4	6.9

(continued on next page)

Table 3 (*continued*)

CK268 muscovite		*J=.0064470 (70.5506909/24.1126245)*								
Temp (°C)	$^{40}Ar/^{39}Ar$	$^{38}Ar/^{39}Ar$	$^{37}Ar/^{39}Ar$	$^{36}Ar/^{39}Ar$	^{39}Ar (mol)$\times 10^{-15}$	$F^{39}Ar$	$\%^{40}Ar^*$	$^{40}Ar^*/^{39}Ar_K$	Age (Ma)	$\pm 1\sigma$
709	46.308	0.01	0.012	7.369	2.00	5.89	95.3	44.11	451.8	0.9
784	44.093	0.012	0.005	8.452	11.80	28.85	94.3	41.58	428.7	0.8
881	41.31	0.011	0.012	0.747	3.01	34.7	99.4	41.07	424.0	0.4
920	41.022	0.01	0.008	0.701	2.72	39.98	99.5	40.80	421.5	0.4
983	41.124	0.012	0.008	0.369	3.71	47.19	99.7	41.00	423.3	0.2
1050	40.897	0.01	0.005	0.165	5.91	58.67	99.8	40.83	421.8	0.2
1113	40.878	0.01	0.003	0.23	10.20	78.53	99.8	40.79	421.4	0.1
1176	40.974	0.009	0.012	0.446	9.00	96.01	99.6	40.82	421.7	0.2
1246	41.719	0.01	0.058	1.067	1.16	99.13	99.2	41.39	427.0	0.3
1296	42.05	0.009	0.136	4.457	0.45	100	96.9	40.73	420.9	1.3
CK009 biotite		*J=.0063960 (70.7343/23.25446667)*								
Temp (°C)	$^{40}Ar/^{39}Ar$	$^{38}Ar/^{39}Ar$	$^{37}Ar/^{39}Ar$	$^{36}Ar/^{39}Ar$	^{39}Ar (mol)$\times 10^{-15}$	$F^{39}Ar$	$\%^{40}Ar^*$	$^{40}Ar^*/^{39}Ar_K$	Age (Ma)	$\pm 1\sigma$
482	38.068	0.151	0.198	64.809	0.41	1.64	49.7	18.92	206.2	3.5
592	56.849	0.164	0.023	78.311	2.13	10.19	59.3	33.69	352.3	15.7
648	41.845	0.175	0	2.515	3.39	23.78	98.2	41.08	421.1	0.5
690	41.146	0.139	0.004	2.518	2.95	35.63	98.1	40.38	414.7	0.4
733	50.444	0.149	0.02	32.084	1.82	42.95	81.2	40.95	419.9	1.8
836	42.18	0.094	0.003	4.591	1.37	48.46	96.7	40.80	418.6	0.5
882	42.815	0.094	0.008	4.795	1.59	54.85	96.6	41.38	423.8	1.4
937	41.785	0.198	0.011	1.636	4.81	74.17	98.8	41.28	423.0	0.5
1011	41.464	0.171	0.013	1.089	2.52	84.26	99.2	41.12	421.5	0.5
1053	41.668	0.21	0.022	0.003	1.81	91.52	100.0	41.65	426.3	0.4
1099	41.671	0.147	0.013	0.533	2.11	100	99.6	41.50	424.9	0.8

Sample locations are given in decimal degrees (WGS84 datum).

pattern from CK206 yields a somewhat irregular spectrum suggesting the presence of excess radiogenic argon. Steps 4–9 (Table 3) yield a weighted mean age of 418±6 Ma accounting for 94% of the gas evolved (Fig. 11C). Excluding the first three low temperature and low gas volume steps, the remaining data spread along an inverse isochron with a $^{40}Ar/^{36}Ar$ intercept of 352±14. The inverse isochron corresponds to an age of 417±8 Ma with an upper intercept above the accepted atmospheric value (Fig. 11C). Statistically, the inverse isochron is not significantly different from the weighted mean age from the spectrum. The isochron age is used in the subsequent discussion as it does not assume an atmospheric trapped ratio.

5.4. CK253

Sample CK253 is from a weakly-deformed pegmatite cutting the intense N–S plunging tectonic fabric in the c. 438 Ma Bakfjord granite (Kirkland et al., 2005a) (Fig. 4F). The pegmatite contains aggregates of large (cm.-scale) undeformed crystals of both biotite and white mica (Fig. 4F). These undeformed white mica grains yield a relatively concordant Ar release spectra with a weighted mean age of 415±6 Ma accounting for 98% of the gas released when three low gas volume steps are discounted (Fig. 11D). An inverse isochron of the same data yields a $^{40}Ar/^{36}Ar$ intercept of 297±17 within error of the accepted atmospheric value (Fig. 11D). The high MSWD of the inverse isochron regression is due to the highly radiogenic nature of the gas released (poorly constrained upper intercept) and the very low analytical uncertainty on the data points. Nevertheless the inverse-isochron age is within error of the weighted mean age, indicating that the plateau is not compromised by the presence of extraneous ^{40}Ar.

5.5. CK268

Sample CK268 was taken from an outcrop of Storelv Schist within the Havvatnet Imbricate Stack. The sample consists of quartz, muscovite, K-feldspar, biotite and accessory phases of monazite and zircon. Large muscovite porphyroblasts (up to 5 mm in length) lie within the foliation and are wrapped by fine-grained biotite defining the penetrative foliation. Muscovite grains were used for Ar–Ar geochronology and yield a broadly concordant release spectrum (Fig 11E) with only small variation from a near plateau in the initial small gas volume steps. Steps 4–12 yield a weighted mean age of 422±6 Ma corresponding

to 94% of the total gas released (Fig. 11E). No inverse isochron can be constructed due to the extremely radiogenic nature of the gas released.

5.6. CK009

Biotite was analysed from sample CK009 from the 438±5 Ma old Engesfjellet granite intruding the Hellefjord Schist on Sørøy (Kirkland et al., 2005a). The granite contains plagioclase, quartz, biotite, titanite and K-feldspar and a significant amount of metamorphic amphibole with subordinate accessory zircon, apatite and garnet. A strong foliation is defined by amphibole and biotite, which are deflected around plagioclase phenocrysts.

The release spectrum shows ages that rise rapidly in the first low temperature steps. Release above 648 °C is more stable although no clear plateau is defined (Fig. 11F). The irregularities in the spectrum caution that there may be disturbance from excess argon. Two populations can be defined (on both isochron and spectrum), that at temperature steps 690–733–836 °C and that at 882–937–1011 °C (Table 3). The two highest temperature steps are hampered by low ^{36}Ar and the influence of the blank and are therefore probably unrealistically old. Considering the spectrum in this way, the first group of lower temperature steps yields a weighted mean spectrum age of 417±6 Ma and an isochron of 416±8 Ma, overlapping on the accepted atmospheric value. However, the inverse isochron has greater scatter than can be attributed to analytical uncertainty alone. For the higher temperature steps (excluding the highest two steps of the experiment) a dominance of slightly older ages is noted, these steps yield a weighted mean of 422±6 Ma and an inverse isochron age of 421±8 Ma

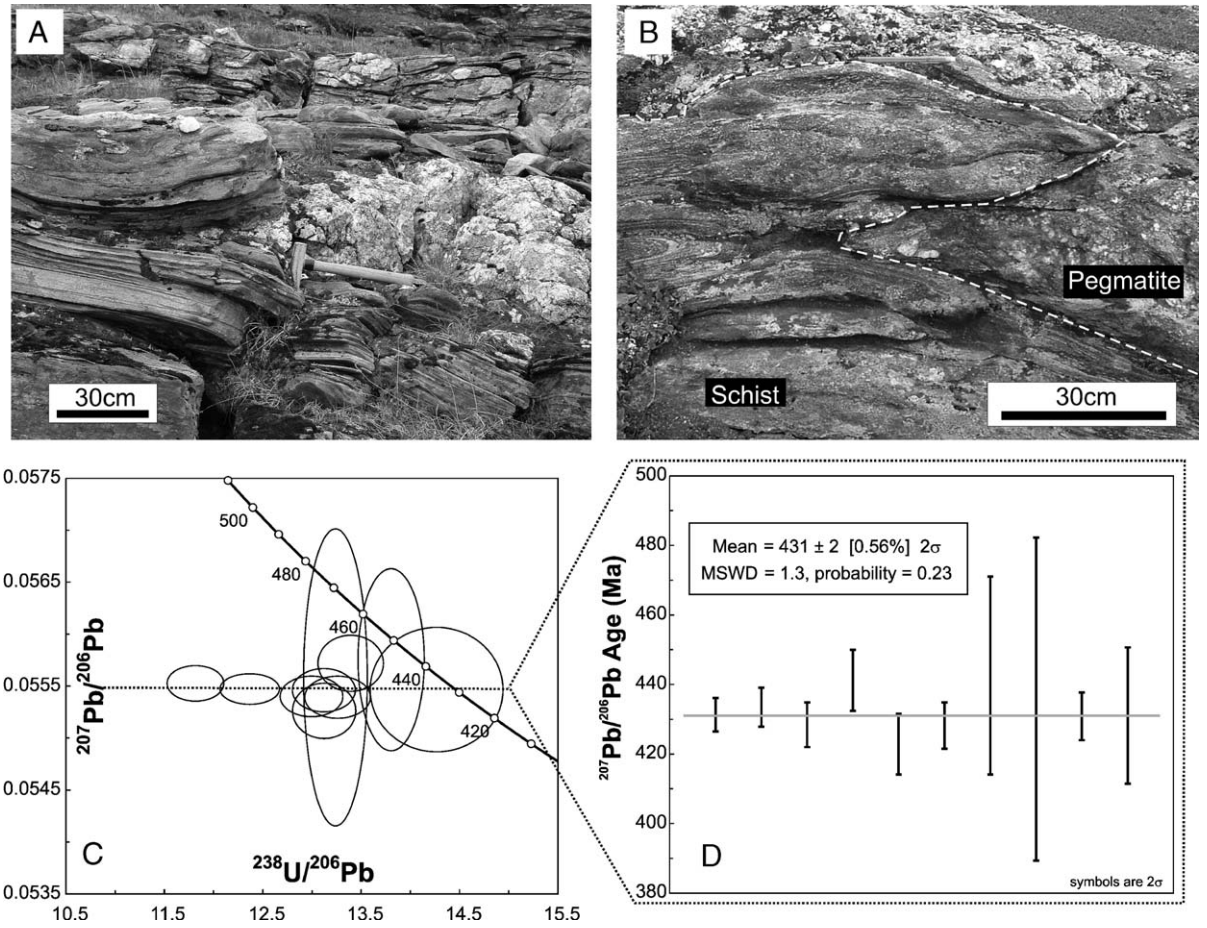

Fig. 12. (A) Pegmatite intruded parallel to the $S0^M$ and $S1^M$ fabrics in the Hellefjord Schist near the Bakfjord Granite (Fig. 1), photographed within 5 m of the CK079 sample site; (B) CK079 pegmatite infolded in $F2^M$ folds with the surrounding Hellefjord Schist; (C) inverse (Tera-Wasserburg) Concordia diagram of zircons from pegmatite sample CK079, deformed by $D2^M$ in the Magerøy Nappe. The reverse discordance is symptomatic of the very high U content; (D) weighted mean $^{207}Pb/^{206}Pb$ age is interpreted as dating crystallization of the pegmatite.

(Fig. 11F). The ordinate intercept on the inverse isochron indicates some excess Ar. The two groups are also observed on the K/Ca and Cl/K plots. Higher apparent Cl in the higher temperature steps may be indicative of Cl-correlated excess argon. Lower temperature steps have lower Cl and higher K/Ca values. We consider the biotite sample to contain two argon reservoirs and that the older of these is likely contaminated by excess argon. The most conservative interpretation would consider the lowest age of the younger group to be least affected by excess argon and provide only a maximum constraint on the cooling age of biotite in this rock at less than c. 415 Ma (Fig. 11F).

6. U–Pb dating, post-D1^{M}, pre-D2^{M} pegmatite

In order to provide further constraint on the timing of the D2^{M} event a granitic pegmatite (CK079), intruding the Hellefjord Schist at Bakfjord, has been dated. The pegmatite intrudes parallel to the bedding and the S1^{M} foliation but is itself folded in F2^{M} folds (Fig. 12A, B). Zircons were extracted by crushing and hand picking. The recovered zircon grains were euhedral, distinctly brown, cathode luminescence-dark and range between 300 and 500 μm in length. The analytical procedure is given in Appendix C.

Ion microprobe analyses (ten spots on eight grains, Fig. 12C, Table 4) yield a consistent $^{207}Pb/^{206}Pb$ age of 431±2 Ma (Fig. 12D), interpreted as dating the crystallization of the pegmatite. The majority of spots are reversely discordant due to the very high U contents (6000–19,000 ppm). The reverse discordance is possibly due to different sputtering behaviour of the sample zircon compared with the lower-U standard, a well documented phenomenon in U-rich zircons (e.g. Wiedenbeck, 1995). Nonetheless the U and Pb concentrations along with the $^{207}Pb/^{206}Pb$ ratio have been accurately determined, benefiting from the high concentrations. The age of this pegmatite constrains D2^{M} to having occurred at or after c. 431 Ma, whereas metamorphic zircon overgrowths on fractured and extruded zircon grains demand that it occurred prior to c. 428 Ma (Kirkland et al., 2005a).

7. Interpretation of geochronology

The fabric relationships of the dated grains to the regional tectonic structures are critical in determining the significance of these results. Samples CK231, CK224 and CK253 have similar relationships to the regional fabrics, i.e., they are developed in post-D2^{M} pegmatites that intruded after the development of the N–S lineation. The undeformed white mica crystals they contain must therefore also post-date the development of the N–S lineation. The $^{40}Ar–^{39}Ar$ ages of these samples are identical within error and yield a weighted mean age of 416±4 Ma (MSWD=0.33). These ages are interpreted as cooling ages as muscovite forming the S2^{M} foliation within the Hellefjord Schist appears to have cooled to its argon retention temperature at an identical time i.e. CK206 417±8 Ma. Cooling ages for muscovite in the Hellefjord Schist are about 6 Ma younger than those recorded in the KNC where typical cooling ages from muscovite fabrics are around 422±2 Ma (n=3, MSWD=1.6; Kirkland et al., 2006b) in agreement with the 423±6 Ma age of large porphyroblastic muscovite from the Storelv Schist dated in this paper (CK268). Excess argon has previously been documented

Table 4
Ion microprobe U–Th–Pb data for sample CK079

Sample / Spot	U (ppm)	Th (ppm)	Pb (ppm)	Th/U	f 206 %	$^{238}U/^{206}Pb$	±σ%	$^{207}Pb/^{206}Pb$	±σ%	% Disc. (2σ)	$^{207}Pb/^{206}Pb$ (Ma)	±σ	$^{206}Pb/^{238}U$ (Ma)	±σ
CK079 Pegmatite cutting Hellefjord Schist [70.8420002 / 24.6839941]														
1a	17281	332	1483	0.019	0.02	12.36762	1.00	0.05547	0.11	14.2	431	2	501	5
1b	19217	322	1724	0.017	0.01	11.81665	1.00	0.05553	0.13	18.8	433	3	524	5
2a	9648	129	786	0.013	0.00	12.99597	1.00	0.05540	0.14	9.1	428	3	478	5
2b	5967	78	472	0.013	0.01	13.39426	1.02	0.05572	0.20	2.1	441	4	464	5
3a	10149	131	819	0.013	0.01	13.12465	1.00	0.05526	0.20	9.0	423	4	473	5
4a	9298	122	743	0.013	0.01	13.26065	1.03	0.05539	0.15	6.9	428	3	469	5
5a	5850	315	450	0.054	0.99	13.80492	1.00	0.05575	0.64	–	443	14	451	4
6a	8862	105	709	0.012	0.17	13.23955	1.00	0.05558	1.05	–	436	23	469	5
7a	11009	152	889	0.014	0.14	13.12114	1.00	0.05546	0.15	7.3	431	3	473	5
8a	8556	116	636	0.014	0.02	14.26689	1.93	0.05547	0.44	–	431	10	437	8

% Disc (2σ) is the age discordance at the closest approach of the error ellipse to Concordia (2σ level). Positive numbers are reversely discordant. All other errors are at the 1σ level. f 206% is the percentage of common ^{206}Pb, estimated from the measured ^{204}Pb. Age calculations use the routines of Ludwig (2003). The sample location is given in decimal degrees (WGS84 datum).

as extensively affecting the KNC (Dallmeyer, 1988; Kirkland et al., 2006b). To a more limited extent it was recorded within the Magerøy Nappe (Kirkland et al., 2006b). Cores of large porphyroblastic biotite within the Hellefjord Schist, as discussed previously, are unaffected by excess radiogenic argon and yielded a inverse isochron age of 401±7 Ma (Kirkland et al., 2006b). This was interpreted as a cooling age. The youngest portion of the release spectrum of CK009 is least affected by excess argon and records an apparent age of 415±1 Ma consistent with an interpretation of biotite cooling through its blocking temperature around c. 400 Ma in the Magerøy Nappe. This is in keeping with the Rb–Sr biotite age for the Engesfjellet Granite of 415±6 Ma (Kirkland et al., 2006b).

7.1. Tectonic significance of mineral lineations in the KNC and Magerøy Nappe

Two mineral lineation directions are apparent within the region, a N–S trend dominant in the Bakfjord and Repvåg granite and a conglomerate unit within the Hellefjord Schist along with a broad E–W trend seen within the Litlefjord and Revsneshamn granites and also displayed in the 'basement' paragneiss (Figs. 1 and 3). Stretching lineations may be considered the result of either the deformation at the end of a sequence of structural modifications or related to a single kinematic cause, as in a simple shear event (Grujic and Mancktelow, 1995).

The east–west trend shows some variation, although it is generally orthogonal to the F2, F3 and F4 fold axes and broad trend of the thrust nappe contact. It is likely that this E–W lineation relates to a single kinematic cause with transport broadly orientated top to the east (Fig. 1).

The tectonic significance of the N–S lineation, constrained to have developed at or after c. 431 Ma and before c. 428 Ma, is more enigmatic. The parallelism between fold axis and mineral lineation direction is common in many orogenic belts (Cloos, 1946; Froitzheim, 1992) and can result from the rotation of folds under non-coaxial deformation. However such a deformation regime would require high strains and would be expected to produce sheath-like geometries in the N–S direction. Typical fold profiles are not sheath-like although within isolated zones of higher strain, sheath folds do occur. However, these have an ENE–WSW axis and are thus likely due to top-to-the-east fold intensification (Fig. 3).

The N–S $D2^M$–$D4^K$ lineation corresponds to approximately 50% shortening in the east–west orientation and is associated with N–S extension. This orientation is anticlockwise of parallelism with the regional fold axis. This indicates departure from plane strain, lying within the constriction field of the finite strain ellipsoid. Near parallelism between fold axis and lineation direction can be created through a transpressive system with pure and simple shear components causing contraction across the zone to be taken up by vertical extension (Harding, 1971; Wilcox et al., 1973). In such a model, folds would develop with axes parallel to the maximum stretching direction with vertical axial planes, with a finite strain ellipse represented by oblate ellipsoids ($K<1$) (Sanderson and Marchini, 1984). However, the presence of a constrictional ellipsoid that has its axis of maximum extension orthogonal to the transport direction suggests that buttressing in the broad E–W direction of Scandian compression occurred during the formation of the N–S directed lineation. It is probable that top-to-the-east compression resulted in some material 'flow' at a high angle to the main orogenic compressional direction.

Transportation paths involving nearly orthogonal changes in direction of relative movement have been described from several orogens. For example, Peterson and Robinson (1993) examined the structural transport directions near the Bronson Hill anticlinorium in the Appalachian orogen, and found a progression from orogen-orthogonal to orogen-parallel transport. Likewise, Merle and Brun (1984) studied the incremental strain history of the Parpaillon Nappe in the French Alps and found evidence for initial NW-directed movement of the nappe followed by SW-directed movement. Within the Efjorden area, some 300 km SW of the present study area, Northrup and Burchfiel (1996) presented structural data that indicated simultaneously disparate directions of tectonic transport. They interpreted the fabrics to mean coeval top-to-the-ESE movement in the allochthon and top-to-the-SSW orogen-parallel movement within the underlying autochthon. A similar situation of deformation partitioning cannot be invoked in the present case as the same nappe contains evidence in the form of the relative age of fold axes, mineral lineations and striations for initial top to the E/ESE transport before N–S orientated motion developed. Orogen-parallel lineations are well developed on the East Greenland side of the Caledonian Orogen. In NE Greenland these lineations are associated with flat-lying folds and top-to-the-north shear (Strachan et al., 1992). In central East Greenland they are prolate and developed at c. 430 Ma during syn-convergent extension (White et al., 2002), a timing very similar to prolate deformation in the Magerøy Nappe (i.e. c. 431–428 Ma).

The strain pattern and the orientation of fabrics, in the KNC and Magerøy Nappe, are most consistent with orogenic compression directed broadly E–W with ESE

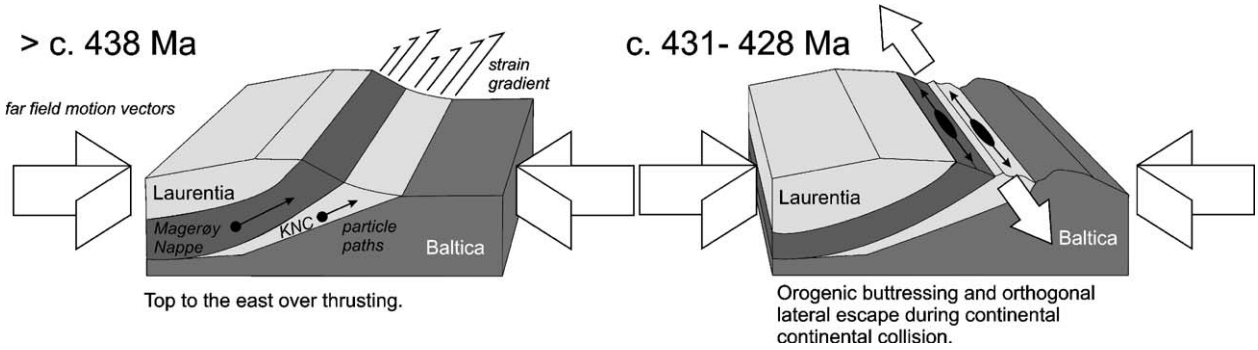

Fig. 13. Cartoon illustrating (left) top to the east over thrusting and tectonic thickening as Laurentia collides with Baltica. Continued collision (right) results in buttressing and lateral escape which occurred in northernmost Norway between c. 431 and 428 Ma. The lateral escape is manifest regionally as a strong N–S mineral lineation and intense prolate strain.

to later E-directed overthrusting. This matured into N–S directed lateral escape, associated with constrictional strain, once the resistance to overthrusting exceeded the yield strength of the rocks and was likely coeval with the full continental–continental stage of the collision (Fig. 13). Thus the direction of mineral lineations and the shape of the associated strain ellipsoid can be used to recognise different stages in the destruction of an ocean and the evolution of a mountain belt.

8. Conclusions

The Scandinavian Caledonides are characterized by a series of major nappes thrust eastwards onto Baltica during the early Palaeozoic closure of the Iapetus Ocean. Various tectonic fabrics within the KNC have been associated with this event, i.e. the Scandian Orogeny *sensu lato* (Zwaan and Roberts, 1978). However distinct phases of this event can be distinguished. One of these is manifest by a N–S mineral lineation and is particularly widespread in both the KNC and Magerøy Nappe. This paper has focused on the cause of this fabric and its timing, hence elucidating the tectonic development within this stage of the collision.

Analysis of clast shapes in a deformed conglomerate affected by this N–S fabric provides the first quantitative estimate of the 3-D strain for this event. Strain analysis using the θ-curve method gives X/Z, Y/Z and X/Y strain ratios (and 95% confidence limit errors) of 5.79 ± 0.86, 1.55 ± 0.24 and 3.89 ± 0.059, respectively. These differ insignificantly from strain estimates using the harmonic mean of clast shapes. A new method is presented to calculate the strain within a conglomerate using linear regressions to model the clast length in all three dimensions. This method allows identification of outliers within the dataset and results in a strain value consistent with all other methods used. All methods suggest prolate deformation. Fry analysis was used to assess the strain within the enclosing psammite matrix yielding similar values, consistent with the lithological similarity of the clasts and matrix. The results indicate c. 50% horizontal shortening parallel to the thrusting direction and c. 200% extension along the orogenic strike.

In order to use strain analysis to constrain tectonic models, it must be combined with a clear distinction of deformation phases. This may be achieved by bracketing fabrics through dating undeformed versus deformed crystal phases. The N–S lineation affecting both the Magerøy Nappe ($D2^M$) and the KNC ($D4^K$) must have developed after c. 438 Ma as zircon grains of this age have been fractured and extruded parallel to the fabric (Kirkland et al., 2005a). Undeformed white micas in pegmatites in the Magerøy Nappe yield Ar–Ar ages of c. 416 Ma. Although these are probably cooling ages, field relationships demonstrate that the N–S lineation must have developed before they grew, which itself occurred before c. 416 Ma and after c. 438 Ma. This is consistent with the lower age constraint of c. 428 Ma reported by Kirkland et al. (2005a) from metamorphic zircon overgrowths on fractured crystals. A precise limit for the $D2^M$ event is provided by the 431 ± 2 Ma age of a deformed pegmatite, which intruded between $D1^M$ and $D2^M$. Hence $D2^M$ (and $D4^K$) took place between c. 428 and 431 Ma.

Collisional forces appear to have driven lateral escape because gravitational collapse, leading to the development of Devonian basins, is a distinctly later event. The development of Devonian basins is recorded throughout Norway soon after 401 Ma (Eide et al., 2002; Kendrick et al., 2004). Hence, horizontal forces induced by continental collision must provide a more effective driving force for lateral extrusion than the gravitational instability of the thickened crust in at least the active stages of collision.

These results indicate that lateral escape was directed nearly orthogonal to the collision vector and occurred during the continent–continent collision stage of the orogeny before gravitational driven collapse (Fig. 13). The field results from this study confirm the orogenic modelling results of Seyferth and Henk (2004), which concluded that orogen-parallel extension is intimately related to continental collision and occurs essentially contemporaneously with convergence.

The orientation and timing of compressional versus extensional stresses can be used as a guide to the phase of the orogeny, i.e., to differentiate between subduction of oceanic material, full continental collision and orogenic collapse. The N–S lineation and its timing are consistent with continental–continental collision causing orogenic buttressing and concomitant orogen-parallel lateral escape. The full continental collision between Baltica and Laurentia occurred after c. 438 Ma, the age of back arc basin sedimentation, and before c. 416 Ma, the Ar–Ar cooling age of white mica. Within the northernmost Norwegian Caledonides a tight constraint on the Scandian collision is placed between c. 431 and 428 Ma.

Acknowledgements

Field and laboratory work were supported by a Government of Ireland (IRCSET) Embark Initiative Postgraduate Research Scholarship awarded to C.L. Kirkland and an IRCSET Basic Research Grant (SC/2002/248) awarded to J.S. Daly. We sincerely thank B. Hendriks and M. Ganerød for assistance in the NGU argon Laboratory. T. Torsvik is thanked for the accommodation at Langstrand. Finally, we would like to thank I. Alsop, M. Steltenpohl and editor J.P. Burg for constructive comments which improved the paper. The Nordsim facility is financed and operated under an agreement between the research councils of Denmark, Norway and Sweden, the Geological Survey of Finland and the Swedish Museum of Natural History. This is Nordsim publication 156.

Appendix A. Sample description

Sample CK060, coordinates: 70.6761807; 23.208 2587 decimal degrees (WGS 84), at Gamnes point, on Sørøy, east of Langstrand (Fig. 1). Matrix-supported monomict conglomerate consisting of weakly-foliated psammite pebbles (quartz, feldspar and minor biotite defining the foliation) in a matrix composed predominantly of quartz, biotite and feldspar with rare muscovite, garnet and fibrolitic sillimanite.

Within the matrix a strong foliation is defined by biotite grains which have a N–S lineation. Biotite also forms large clots in the matrix consisting of several grains (up to 3 mm long). The sample is strongly deformed, showing constrictional strain (see Figs. 4 and 10). In general, the matrix exhibits a blastomylonitic fabric, with a coarse equigranular polygonal texture within the strongly stretched pebbles. Very rarely a very fine-grained equigranular quartzo-feldspathic mantle is present on the outer margin of the psammite clasts.

Appendix B. Rf/φ method

During deformation, an elliptical passive marker will be transformed to a new shape with aspect ratios Rf and long axis orientation, φ, dependant on the original shape (Ri) and orientation (θ) of the marker and the shape (Rs) and orientation of the strain ellipse. The quantities Rf and φ can be measured directly from the deformed clast. Accepting some simplifying assumptions, the influence of the four parameters that control the final distribution of Rf and φ can be determined.

One assumption is that the ellipsoids were originally randomly oriented, leading to symmetric patterns of data on Rf/φ diagrams (Ramsay and Huber, 1983). Statistical methods can be used to test this (Lisle, 1985). In the case of randomly orientated clasts, the orientation of the maximum principal stretching direction is the orientation that bisects the data. The basis of this method is as follows: prior to deformation the elliptical strain marker makes an angle, (θ) between its long axis and the X direction of the strain ellipsoid. The markers have an ellipticity and different initial orientations. After deformation, however, the strain markers have a modified ellipticity (Rf) and now make a different angle (φ) between their long axis and the maximum extension direction. The strain ellipse is then calculated by unstraining the markers until they have a shape and orientation, which would be expected to have existed in the rock before it was strained.

A variety of methods can be used to estimate the strain ratio from Rf/φ diagrams. Ramsay and Huber (1983) suggest using the maximum and minimum values of Rf to determine the strain ratio. However, a more elegant solution, which also provides a quantitative method to estimate the errors is provided by Lisle (1977). Marker ellipses with the same initial orientation (θ) but with a range of aspect ratios define a series of curves on an Rf/φ diagram, (θ-curves) that depend only on the strain ratio (Lisle, 1977). Sets of θ-curves can be drawn in Rf/φ space for a series of different initial orientations. The strain ratio (Rs) that best accounts for a set of Rf/φ data is

determined by comparing the Rf/φ data with θ-curves. R is then found from the θ-curve which produces the best fit to the data (Fig. 6). The χ^2 test (Lisle, 1985) is used to evaluate the goodness of fit and provides a method to estimate the errors.

Appendix C. Geochronology methods

Ar–Ar procedure

All samples were crushed and sieved prior to hand-picking under a binocular microscope. High-purity mineral separates of muscovite and biotite (CK009) were produced. Mineral separates were washed in distilled water and acetone prior to packing in Al foil for irradiation.

The mineral separates were irradiated in a single batch at the McMaster research reactor, Hamilton, Canada. Rio Tinto biotite (410.3 Ma) and Sanidine TCR (Taylor Creek 28.3 Ma) and FCT biotite (Fish Canyon 28.0 Ma) along with K and Ca salts, were irradiated with the samples as monitors to determine the J value.

All Ar measurements were made at the Norwegian Geological Survey argon laboratory by resistance furnace step-heating. Temperature increments were typically 50 °C. Blanks had a near atmospheric composition and accounted for <1–5% of the ^{40}Ar and less than 1% of the ^{36}Ar, ^{37}Ar, ^{38}Ar and ^{39}Ar released. Blank corrections were applied based on a daily blank. Mass discrimination values were determined on measured atmospheric ^{40}Ar/^{36}Ar from an air pipette. Analytical protocols follow Eide et al. (2005, 2002). Standard corrections were made for ^{37}Ar decay after irradiation and Ar interference reactions based on measured ^{36}Ar/^{37}Ar (Ca)=0.000285; ^{39}Ar/^{37}Ar (Ca)=0.000724 and ^{40}Ar/^{39}Ar (K)=0.01923 values determined from the K and Ca salts.

U–Th–Pb procedure

Zircons were extracted from the sample by crushing, sieving, heavy liquid and hand picking. About 50 grains were mounted in epoxy resin and polished to reveal the grain interiors. Grains were imaged under reflected light and by cathodoluminescence to determine the internal structure. Determination of Pb/U, Pb/Pb isotope ratios and U, Th, and Pb concentrations were performed on a Cameca IMS 1270 ion microprobe at the Swedish Museum of Natural History. The analytical procedure follows Whitehouse et al. (1999), using 91500 zircon as the U/Pb ratio calibration standard.

References

Aitcheson, S.J., 1990. Nd isotopic evidence for exotic detritus in the Kalak Nappe Complex, north Norwegian Caledonides. Journal of the Geological Society, London 147, 923–926.

Alsop, G.I., Bryson, R., Hutton, D.H.W., 2001. Tectonic and kinematic evolution within mid-crustal orogenic root zones: a study from the Caledonides of Northwestern Ireland. Geological Magazine 138, 193–211.

Andersen, T.B., 1981. The structure of the Magerøy nappe, Finnmark, North Norway. Norges Geologiske Undersokelse, Bulletin 363, 1–23.

Andersen, T.B., 1984. The stratigraphy of the Magerøy Supergroup, Finnmark, North Norway. Norges Geologiske Undersøkelse, Bulletin 395, 25–38.

Andersen, T.B., 1989. A comment: alternative to the Finnmarkian–Scandian interpretation on Magerøya, northern Norway. Norsk Geologisk Tidsskrift 69, 291–294.

Andersen, T.B., Austrheim, H., Sturt, B.A., Pedersen, S., Kjærsrud, K., 1982. Rb–Sr whole rock ages from Magerøy, North Norwegian Caledonides. Norsk Geologisk Tidsskrift 2, 79–85.

Andréasson, P.G., 1994. The Baltoscandian margin in Neoproterozoic–early Palaeozoic times. Some constraints on terrane derivation and accretion in the Arctic Scandinavian Caledonides. Tectonophysics 231, 1–32.

Andréasson, P.G., Gee, D.G., Whitehouse, M.J., Schöberg, H., 2003. Subduction-flip during Iapetus Ocean closure and Baltica–Laurentia collision, Scandinavian Caledonides. Terra Nova 15, 362–369.

Andresen, A., Hartz, E.H., Vold, J., 1998. A late orogenic extensional origin for the infracrustal gneiss domes of the East Greenland Caledonides (72–74°N). Tectonophysics 285, 353–369.

Binns, R.E., 1989. Regional correlations in NE Troms– W Finnmark: the demise of the "Finnmarkian" orogeny? In: Gayer, R.A. (Ed.), The Caledonide Geology of Scandinavia. Graham and Trotman, London, pp. 27–45.

Borradaile, G.J., Johnson, H.D., 1973. Finite strain estimates from the Dalradian dolomitic formation, Islay, Argyll, Scotland. Tectonophysics 18 (3–4), 249.

Braathen, A., Nordgulen, Ø., Osmundsen, P.T., Andersen, T.B., Solli, A., Roberts, D., 2000. Devonian, orogen-parallel, opposed extension in the Central Norwegian Caledonides. Geology 28, 615–618.

Chapman, T.J., Milton, N.J., Williams, G.D., 1979. Shape fabric variations in deformed conglomerates at the base of the Laksefjord Nappe, North Norway. Journal of the Geological Society, London 136, 683–689.

Chapman, T.J., Gayer, R.A., Williams, G.D., 1985. Structural cross-sections through the Finnmark Caledonides and timing of the Finnmark event. In: Gee, D.G., Sturt, B.A. (Eds.), The Caledonide Orogen.

Chauvet, A., Seranne, M., 1994. Extension-parallel folding in the Scandinavian Caledonides: implications for late-orogenic processes. Tectonophysics 238, 31–54.

Chauvet, A., Kienast, J.R., Pinardon, J.L., Brunel, M., 1992. Petrological constraints and PT path of Devonian collapse tectonics within the Scandian mountain belt (Western Gneiss region, Norway). Journal of the Geological Society, London 149, 383–400.

Chew, D.M., 2003. An Excel spreadsheet for finite strain analysis using the Rf/Phi technique. Computers & Geosciences 29, 795–799.

Cloos, E., 1946. Lineation. A critical review and annotated bibliography. Memoirs of the Geological Society of America 18, 122.

Corfu, F., Roberts, R.J., Torsvik, T.H., Andersen, T.B., Ramsay, D.M., Ashwal, L.D., 2004. Crustal processing: the Finnmarkian orogen reassessed. Geochimica et Cosmochimica Acta 68, A624.

Corfu, F., Roberts, R.J., Gerber, M., Torsvik, T.H., Andersen, A., Ramsay, D.M., Ashwal, L.D., 2005. Exotic terranes in the Finnmark Caledonides: U–Pb evidence for Peri-Gondwanan and Laurentian elements. Norwegian Geological Winter meeting, Røros, Abstract and Proceedings. No. 1:22, p. 22.

Corfu, F., Torsvik, T.H., Andersen, A., Ashwal, L.D., Ramsay, D.M., Roberts, R.J., 2006. Early Silurian mafic–ultramafic and granitic plutonism in contemporaneous flysch, Magerøy, northern Norway: U–Pb ages and regional significance. Journal of the Geological Society, London 163, 291–301.

Dallmeyer, R.D., 1988. Polyorogenic $^{40}Ar/^{39}Ar$ mineral age record within the Kalak Nappe Complex, Northern Scandinavian Caledonides. Journal of the Geological Society, London 145, 705–716.

Dallmeyer, R.D., Reuter, A., 1989. $^{40}Ar/^{39}Ar$ whole rock dating and the age of cleavage in the Finnmark autochthon, northernmost Scandinavian Caledonides. Lithos 22, 213–227.

Daly, J.S., Aitcheson, S.J., Cliff, R.A., Gayer, R.A., Rice, A.H.N., 1991. Geochronological evidence from discordant plutons for a late Proterozoic orogen in the Caledonides of Finnmark, northern Norway. Journal of the Geological Society, London 148, 29–40.

Dangla, P., Demange, A.P., Quenardel, J.-M., Sonet, J., 1978. Données géochronologiques sur les Calédonides scandinaves septentrolales (Troms, Norvège du Nord). Comptes Rendus l'Académıe des Sciences (Paris) 286, 1653–1656 (in French).

Dickinson, W.R., 1976. Sedimentary basins developed during evolution of Mesozoic–Cenozoic arc-trench systems in western North America. Canadian Journal of Earth Sciences 13, 1268–1287.

Dunnet, D., 1969. A technique of finite strain analysis using elliptical particles. Tectonophysics 7, 117–136.

Dunning, G.R., Pedersen, R.B., 1988. U/Pb ages of ophiolites and arc related plutons of the Norwegian Caledonides: implications for the development of the Iapetus. Contributions to Mineralogy and Petrology 98, 13–23.

Eide, E.A., Osmundsen, P.T., Meyer, G.B., Kendrick, M.A., Corfu, F., 2002. The Nesna Shear Zone, North Central Norway: an $^{40}Ar/^{39}Ar$ record of Early Devonian–Early Carboniferous ductile extension and unroofing. Norwegian Journal of Geology 82, 317–339.

Eide, E.A., Haabsland, N.E., Osmundsen, P.T., Andersen, T.B., Roberts, D., Kendrick, M.A., 2005. Modern techniques and Old Red problems — determining the age of continental sedimentary deposits with $^{40}Ar/^{39}Ar$ provenance analysis in west-central Norway. Norwegian Journal of Geology 85, 133–149.

Flinn, D., 1962. On folding during three-dimensional progressive deformation. Journal of the Geological Society, London 118, 385–433.

Fossen, H., Dunlap, W.J., 1998. Timing and kinematics of Caledonian thrusting and extensional collapse, southern Norway: evidence form $^{40}Ar/^{39}Ar$ thermochronology. Journal of Structural Geology 20, 765–781.

Freeman, B., Lisle, R.J., 1987. The relationship between tectonic strain and the three dimensional shape fabrics of pebbles in deformed conglomerates. Journal of the Geological Society, London 144, 635–639.

Froitzheim, N., 1992. Formation of recumbent folds during synorogenic crustal extension (Austroalpine nappes, Switzerland). Geology 20, 923–926.

Fry, N., 1979. Random point distributions and strain measurement in rocks. Tectonophysics 60, 806–807.

Gayer, R.A., Roberts, D., 1971. The structural relationships of the Caledonian Nappes of Porsangerfjord, West Finnmark, North Norway. Norges Geologiske Undersøkelse Bulletin 269, 21–67.

Gayer, R.A., Humphreys, R.J., Binns, R.E., Chapman, T.J., 1984. Tectonic modelling of the Finnmarkian and Troms Caledonides based on high level igneous geochemistry. In: Gee, D.G., Sturt, B.A. (Eds.), The Caledonide Orogen— Scandinavia and Related areas. John Wiley, London.

Gayer, R.A., Hayes, S.J., Rice, A.H.N., 1985. The structural development of the Kalak Nappe Complex of eastern and Central Porsangerhalvøya, Finnmark, Norway. Norges Geologiske Undersøkelse Bulletin 400, 67–87.

Gayer, R.A., Rice, A.H.N., Roberts, D., Townsend, C., Welbon, A., 1987. Restoration of the Caledonian Baltoscandian margin from balanced cross sections: the problems of excess continental crust. Transactions of the Royal Society of Edinburgh. Earth Sciences 78, 197–217.

Gee, D.G., 1975. A tectonic model for the central part of the Scandinavian Caledonides. American Journal of Science 275, 468–515 (A).

Grujic, D., Mancktelow, N.S., 1995. Folds with axes parallel to the extension direction: an experimental study. Journal of Structural Geology 17, 279–291.

Hacker, B.R., Gans, P.B., 2005. Continental collisions and the creation of ultrahigh-pressure terranes: Petrology and thermochronology of nappes in the central Scandinavian Caledonides. GSA Bulletin 117, 117–134.

Harding, T.P., 1971. Tectonic transpression in Caledonian Spitzbergen. Geology Magazine 108, 27–42.

Henningsmoen, G., 1961. Cambro-Silurian fossils in Finnmark, northern Norway. Norges Geologiske Undersøkelse Bulletin 213, 93–95.

Kendrick, M.A., Eide, E.A., Roberts, D., Osmundsen, P.T., 2004. The Middle to Late Devonian Høybakken detachment, central Norway: $^{40}Ar–^{39}Ar$ evidence for prolonged late/post-Scandian extension and uplift. Geological Magazine 141, 329–344.

Kirkland, C.L., Daly, J.S., Whitehouse, M.J., 2005a. Early Silurian magmatism and the Scandian evolution of the Kalak Nappe Complex Finnmark, Arctic Norway. Journal of the Geological Society, London 162, 985–1003.

Kirkland, C.L., Daly, J.S., Eide, E., Whitehouse, M.J., 2005b. Tectonic events in the Kalak Nappe Complex, Arctic Caledonides redefined through a linked structural and geochronological approach. Geophysical Research Abstracts 7, 10097.

Kirkland, C.L., Daly, J.S., Whitehouse, M.J., 2006a. Granitic magmatism of Grenvillian and late Neoproterozoic age in Finnmark, Arctic Norway:— constraining pre Scandian deformation in the Kalak Nappe Complex. Precambrian Research 145, 24–52.

Kirkland, C.L., Daly, J.S., Eide, E.A., Whitehouse, M.J., 2006b. Tectonic evolution of the Arctic Norwegian Caledonides from a texturally- and structurally-constrained multi-isotopic (Ar–Ar, Rb–Sr, Sm–Nd, U–Pb) study. American Journal of Science (In review).

Kirkland, C.L., Daly, J.S., Whitehouse, M.J., in press. Provenance and terrane evolution of the Kalak Nappe Complex, Norwegian Caledonides: implications for Neoproterozoic palaeogeography and tectonics. Journal of Geology 115.

Kjærsrud, K., 1985. The geology of the north-western Magerøy, Finnmark, with special reference to the Caledonian tectonometamorphic evolution. PhD Thesis, University of Bergen.

Krabbendam, M., Dewey, J.F., 1998. Exhumation of UHP rocks by transtension in the Western Gneiss region, Scandinavian Caledonides. In: Holdsworth, R.E., Strachan, R.A., Dewey, J.F. (Eds.),

Continental Transpressional and Transtensional Tectonics. Geological Society, London, Special Publications, vol. 135, pp. 159–181.

Krill, A.G., Zwaan, B., 1987. Reinterpretation of Finnmarkian deformation on western Sørøy, northern Norway. Norsk Geologisk Tidsskrift 67, 15–24.

Krill, A.G., Rodgers, J., Sundvoll, B., 1988. Alternative to the Finnmarkian–Scandian interpretation on Magerøya, northern Norway. Norsk Geologisk Tidsskrift 68, 171–185.

Krill, A.G., Marek, J., Kunst, M., Storch, P., 1993. Middle Llandovery (Lower Aeronian) graptolites from hornfels on Magerøya. Geonytt 1, 28.

Law, R.D., 1986. Relationship between strain and quartz crystallographic fabrics in the Roche Maurice quartzites of Plougastel, western Brittany. Journal of Structural Geology 8, 493–515.

Lisle, R.J., 1977. Clastic grain shape and orientation in relation to cleavage from the Aberystwyth Grits, Wales. Tectonophysics 39, 381–395.

Lisle, R.J., 1985. Geological strain analysis: a manual for the Rf–phi technique. A. Wheaton, Exeter, 99 pp.

Lode, W., 1926. Versuche über den Einfluß der mittleren Hauptspannung auf das Fließen des Metalle Eisen, Kupfer, und Nickel. Zeitschrift Fur Physik 36, 913–939 (in German).

Ludwig, K.R., 2003. User's Manual for Isoplot 3.00 A Geochronological Toolkit for Microsoft Excel. Berkeley Geochronology Center Special Publication, vol. 4.

Melezhik, V.A., Gorokhov, I.M., Fallick, A.E., Roberts, D., Kuznetsov, A.B., Zwaan, K.B., Pokrovsky, B.G., 2002. Isotopic stratigraphy suggests Neoproterozoic ages and Laurentian ancestry for high-grade marbles from the North-Central Norwegian Caledonides. Geological Magazine 139, 375–393.

Merle, O., Brun, J.P., 1984. The curved translation path of the Parpaillon Nappe (French Alps). Journal of Structural Geology 6, 711–719.

Miller, M.M., 1989. Intra-arc sedimentation and tectonism: Late Paleozoic evolution of the eastern Klamath terrane, California. Bulletin of the Geological Society of America 101, 170–187.

Mitchell, A., 1999. The Esri Guide to GIS Analysis. ESRI, Inc., California. 250 pp.

Nadai, A., 1963. Theory of Flow and Fracture of Solids. Engineering Societies Monographs, vol. 2. McGraw–Hill, New York. 572 pp.

Neves, S.P., da Silva, J.M.R., Mariano, G., 2005. Oblique lineations in orthogneisses and supracrustal rocks: vertical partitioning of strain in a hot crust (eastern Borborema Province, NE Brazil). Journal of Structural Geology 27, 1513.

Nordgulen, Ø., Bickford, M.E., Nissen, A.L., Wortman, G.L., 1993. U–Pb zircon ages from the Bindal Batholith and the tectonic history of the Helgeland Nappe Complex, Scandinavian Caledonides. Journal of the Geological Society, London 150, 771–783.

Northrup, C.J., 1997. Timing structural assembly, metamorphism, and cooling of Caledonian Nappes in the Ofoten–Efjorden Area, North Norway: tectonic insights from U–Pb and $^{40}Ar/^{39}Ar$ geochronology. Journal of Geology 105, 565–582.

Northrup, C.J., Burchfiel, B.C., 1996. Orogen-parallel transport and vertical partitioning of strain during oblique collision, Efjorden, north Norway. Journal of Structural Geology 18, 1231–1244.

Osmundsen, P.T., Braathen, A., Nordgulen, Ø., Roberts, D., Meyer, G., Eide, E., 2003. The Devonian Nesna Shear Zone, north-central Norwegian Caledonides, and its regional implications. Journal of the Geological Society, London 160, 137–150.

Pedersen, R.B., Furnes, H., 1991. Geology, magmatic affinity and geotectonic environment of some Caledonian ophiolites in Norway. Journal of Geodynamics 13, 183–203.

Pedersen, R.B., Bruton, D.L., Furnes, H., 1992. Ordovician faunas, island arcs and ophiolites in the Scandinavian Caledonides. Terra Nova 4, 217–222.

Peterson, V.L., Robinson, P., 1993. Progressive evolution from uplift to orogen-parallel transport in a late-Acadian upper amphibolite- to granulite-facies shear zone, south-central Massachusetts. Tectonics 12, 550–567.

Ramberg, H., 1980. Diapirism and gravity collapse in the Scandinavian Caledonides. Journal of the Geological Society, London 137, 261–270.

Ramsay, J.G., 1967. Folding and Fracturing of Rocks. McGraw–Hill, New York. 568 pp.

Ramsay, D.M., 1971. Stratigraphy of Sørøy: in the Caledonian Geology of Northern Norway. Norges Geologiske Undersøkelse Bulletin 269, 314–317.

Ramsay, J.G., Huber, M.I., 1983. The techniques of modern structural geology, 1. Strain Analysis. Academic Press, New York.

Rice, A.H.N., 1984. The significance of a thrust fault lineation in the Kalak Nappe Complex of Finnmark. Norsk Geologisk Tidsskrift 64, 173–180.

Rice, A.H.N., 1987. Continuous out-of-sequence ductile thrusting in the Norwegian Caledonides. Geological Magazine 124 (3), 249–260.

Roberts, D., 1968. Hellefjord Schist Group— a probable turbidite formation from the Cambrian of Sørøy, West Finnmark. Norges Geologiske Undersøkelse Bulletin 48, 231–244.

Roberts, D., 1985. The Caledonian fold belt in Finnmark: a synopsis. Norges Geologiske Undersøkelse Bulletin 403, 161–178.

Roberts, D., 2003. The Scandinavian Caledonides; event chronology, palaeogeographic settings and likely modern analogues. Tectonophysics 1–17.

Roberts, D., Gee, D.G., 1985. An introduction to the structure of the Scandinavian Caledonides. In: Gee, D.G., Sturt, B.A. (Eds.), The Caledonide Orogen — Scandinavia and Related Areas. John Wiley and Sons, Chichester, pp. 55–68.

Roberts, D., Melezhik, V.A., Heldal, T., 2002. Carbonate formations and early NW directed thrusting in the highest allochthons of the Norwegian Caledonides: evidence of a Laurentian ancestry. Journal of the Geological Society, London 159, 117–120.

Roberts, R.J., Corfu, F., Torsvik, T.H., Ramsay, D.M., Ashwal, L.D., 2004. Redefining the magmatic evolution of the Kalak Nappe Complex. Geologiska Föreningen i Stockholm. Abstract Volume, 26th Nordic Geological Winter Meeting 126, 84.

Robins, B., 1998. The mode of emplacement of the Honningsvåg Intrusive Suite, Magerøya, northern Norway. Geological Magazine 135, 231–244.

Robins, B., Gardner, P.M., 1975. The magmatic evolution of the Seiland Province, and Caledonian plate boundaries in northern Norway. Earth and Planetary Science Letters 26, 167–178.

Sanderson, D.J., Marchini, W.R.D., 1984. Transpression. Journal of Structural Geology 6, 449–458.

Seguret, M., Seranne, M., Chauvet, A., Brunel, M., 1989. Collapse basin; a new type of extensional sedimentary basin from the Devonian of Norway. Geology 17, 127–130.

Seno, S., Dallagiovanna, G., Vanossi, M., 1998. From finite strain data to strain history: a model for a sector of the Ligurian Alps, Italy. Journal of Structural Geology 20, 573–585.

Seyferth, M., Henk, A., 2004. Syn-convergent exhumation and lateral extrusion in continental collision zones—insights from three-dimensional numerical models. Tectonophysics 382, 1–29.

Shaw, S.L., Salmon, E.D., Quatrano, R.S., 1995. Digital photography for the light microscope: results with a gated, video-rate CCD Camera and NIH-Image Software. BioTechniques 19, 946–955.

Siedlecka, A., Roberts, D., 1996. Finnmark Fylke Berggrunnsgeologi. Norges Geologiske Undersøkelse.

Slagstad, T., Melezhik, V.A., Kirkland, C.L., Zwaan, K.B., Roberts, D., Gorokhov, I.M., Fallick, A.E., 2006. Carbonate isotope chemostratigraphy suggests revisions to the geological history of the West Finnmark Caledonides, North Norway. Journal of the Geological Society, London 163, 277–289.

Steltenpohl, M.G., Andresen, A., Linstrøm, M., Gromet, P., Steltenpohl, L.W., 2003. The role of felsic and mafic igneous rocks in deciphering the evolution of thrust-stacked terranes: an example from the north Norwegian Caledonides. American Journal of Science 303, 149–185.

Strachan, R.A., Holdsworth, R.E., Friderichsen, J.D., Jepsen, H.F., 1992. Regional Caledonian structure within an oblique convergence zone, Dronning Louise Land, NE Greenland. Journal of the Geological Society, London 149, 359–371.

Strine, M., 2003. Implications of three-dimensional thrust surface geometry on thrust sheet kinematics; a study along the Moine Thrust, NW Scotland. Geological Society of America Abstracts with Programs 35, 603.

Sturt, B.A., Pringle, I.R., Ramsay, D.M., 1978. The Finnmarkian phase of the Caledonian orogeny. Journal of the Geological Society, London 135, 597–610.

Townsend, C., 1986. Thrust tectonics within the Caledonides of Northern Norway. PhD. Thesis, University of Wales.

Townsend, C., 1987. Thrust transport directions and thrust sheet restoration in the Caledonides of Finnmark, North Norway. Journal of Structural Geology 9, 345–352.

Treagus, S.H., Treagus, J.E., 2002. Studies of strain and the rheology of conglomerates. Journal of Structural Geology 24, 1541–1567.

Vaasjoki, M., Sipila, P., 2001. U–Pb Isotopic determinations on baddeleyite and zircon from the Halti–Ridnitsohkka in Finnish Lapland: a further constraint on Caledonide evolution. In: Vaasjoki, M. (Ed.), Radiometric age determinations from Finnish Lapland and their bearing on the timing of Precambrian volcano-sedimentary sequences. Geological Survey of Finland Special Paper, vol. 33, pp. 247–253.

White, A., Hodges, K., Martin, M., Andresen, A., 2002. Geologic constraints on middle-crustal behavior during broadly synorogenic extension in the central East Greenland Caledonides. International Journal of Earth Sciences 91, 187–208.

Whitehouse, M.J., Kamber, B.S., Moorbath, S., 1999. Age significance of U–Th–Pb zircon data from Early Archaean rocks of west Greenland: a reassessment based on combined ion-microprobe and imaging studies. Chemical Geology. Isotope Geoscience Section 160, 201–224.

Wiedenbeck, M., 1995. An example of reverse discordance during ion microprobe zircon dating: an artifact of enhanced ion yields from a radiogenic labile Pb. Chemical Geology 125, 197–218.

Wilcox, R.E., Harding, T.P., Seely, D.R., 1973. Basic wrench tectonics. Bulletin of the American Association of Petroleum Geologists 57, 74–96.

Williams, G.D., Chapman, T.J., Milton, N.J., 1984. Generation and modification of finite strain patterns by progressive thrust faulting in the Laksefjord Nappe. Tectonophysics 107, 177–186.

Yoshinobu, A.S., Barnes, C.G., Nordgulen, Ø., Prestvik, T., Fanning, M., Pedersen, R.B., 2002. Ordovician magmatism, deformation, and exhumation in the Caledonides of central Norway: an orphan of the Taconic orogeny? Geology 30, 883–886.

Yoshinori, M., Wallis, S., 2002. Three-dimensional finite strain analysis in the high-grade part of the Sanbagawa Belt using deformed meta-conglomerate. The Island Arc 11, 111–121.

Zachrisson, E., 1986. Scandinavian Caledonides. Stratabound Sulphides., Ba no. 42. Sver. Geol. Unders. Ser.

Zwaan, B., Roberts, D., 1978. Tectonostratigraphic successions and development of the Finnmarkian nappe sequence, North Norway. Norges Geologiske Undersøkelse Bulletin 343, 53–71.